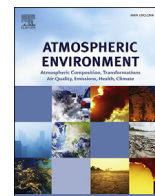




Contents lists available at ScienceDirect

Atmospheric Environment

journal homepage: www.elsevier.com/locate/atmosenv

Source sector and region contributions to concentration and direct radiative forcing of black carbon in China

Ke Li ^{a, b}, Hong Liao ^{a, *}, Yuhao Mao ^a, David A. Ridley ^c

^a State Key Laboratory of Atmospheric Boundary Layer Physics and Atmospheric Chemistry (LAPC), Institute of Atmospheric Physics, Chinese Academy of Sciences, Beijing 100029, China

^b University of Chinese Academy of Sciences, Beijing 100049, China

^c Department of Civil and Environmental Engineering, Massachusetts Institute of Technology, Cambridge, MA, USA

HIGHLIGHTS

- Contributions from five domestic sectors and emissions outside China are simulated.
- Residential and industry sectors are the largest contributors to BC levels in China.
- The TOA direct radiative forcing of BC in China is simulated to be 1.22 W m^{-2} in 2010.
- Domestic and non-China emissions contribute 75% and 25% to BC forcing, respectively.

ARTICLE INFO

Article history:

Received 9 February 2015

Received in revised form

27 May 2015

Accepted 9 June 2015

Available online 12 June 2015

Keywords:

Black carbon

Direct radiative forcing

Sector contribution

Transboundary transport

ABSTRACT

We quantify the contributions from five domestic emission sectors (residential, industry, transportation, energy, and biomass burning) and emissions outside of China (non-China) to concentration and direct radiative forcing (DRF) of black carbon (BC) in China for year 2010 using a nested-grid version of the global chemical transport model (GEOS-Chem) coupled with a radiative transfer model. The Hemispheric Transport of Air Pollution (HTAP) anthropogenic emissions of BC for year 2010 are used in this study. Simulated surface-layer BC concentrations in China have strong seasonal variations, which exceed $9 \mu\text{g m}^{-3}$ in winter and are about $1\text{--}5 \mu\text{g m}^{-3}$ in summer in the North China Plain and the Sichuan Basin. Residential sector is simulated to have the largest contribution to surface BC concentrations, by $5\text{--}7 \mu\text{g m}^{-3}$ in winter and by $1\text{--}3 \mu\text{g m}^{-3}$ in summer, reflecting the large emissions from winter heating and the enhanced wet deposition during summer monsoon. The contribution from industry sector is the second largest and shows relatively small seasonal variations; the emissions from industry sector contribute $1\text{--}3 \mu\text{g m}^{-3}$ to BC concentrations in the North China Plain and the Sichuan Basin. The contribution from transportation sector is the third largest, followed by that from biomass burning and energy sectors. The non-China emissions mainly influence the surface-layer concentrations of BC in western China; about 70% of surface-layer BC concentration in the Tibet Plateau is attributed to transboundary transport. Averaged over all of China, the all-sky DRF of BC at the top of the atmosphere (TOA) is simulated to be 1.22 W m^{-2} . Sensitivity simulations show that the TOA BC direct radiative forcings from the five domestic emission sectors of residential, industry, energy, transportation, biomass burning, and non-China emissions are 0.44, 0.27, 0.01, 0.12, 0.04, and 0.30 W m^{-2} , respectively. The domestic and non-China emissions contribute 75% and 25% to BC DRF in China, respectively. These results have important implications for taking measures to reduce BC emissions to mitigate near-term climate warming and to improve air quality in China.

© 2015 The Authors. Published by Elsevier Ltd. This is an open access article under the CC BY-NC-ND license (<http://creativecommons.org/licenses/by-nc-nd/4.0/>).

1. Introduction

Black carbon (BC) is an important component of aerosols in the atmosphere emitted from incomplete combustion of fossil fuel, biofuel, and biomass (Bond et al., 2013). BC emissions in China

* Corresponding author.

E-mail address: hongliao@mail.iap.ac.cn (H. Liao).

accounted for about 25% of the annual global total emission of BC in recent years (Cooke et al., 1999; Bond et al., 2004; Qin and Xie, 2012; Wang et al., 2012). The annual mean surface-layer BC concentrations were measured to be about $11.2 \mu\text{g m}^{-3}$ at the urban sites, $3.6 \mu\text{g m}^{-3}$ at the rural sites, and $0.35 \mu\text{g m}^{-3}$ at the remote background sites (Zhang et al., 2008). Measured BC concentrations during heavily polluted events reached up to $19.8 \mu\text{g m}^{-3}$ in Xi'an in January, 2013 (Zhang et al., 2015). Black carbon as an air pollutant has harmful impacts on human health (Anenberg et al., 2011; Janssen et al., 2012), and it also plays an important role in climate change through its strong absorption of sunlight (Bond et al., 2013; Intergovernmental Panel on Climate Change (IPCC), 2013).

IPCC (2013) reported that the global and annual mean radiative forcing value of BC was $0.40 (0.05\text{--}0.80) \text{ W m}^{-2}$ between years 1750 and 2011. Regional and global modeling studies have shown that BC radiative forcing over China is much higher than the global mean value reported by IPCC (2013). Wu et al. (2008) reported, by using the Regional Climate Model version 3 (RegCM3), that the average BC direct radiative forcing (DRF) over eastern China ($20^{\circ}\text{--}50^{\circ}\text{N}$, $100^{\circ}\text{--}130^{\circ}\text{E}$) was 1.1 W m^{-2} at the top of the atmosphere (TOA) during 1993–2003. Zhuang et al. (2011), by using the Regional Climate Chemistry Modeling System (RegCCMs), estimated that the annual mean TOA BC DRF over eastern China ($25^{\circ}\text{--}45^{\circ}\text{N}$, $100^{\circ}\text{--}130^{\circ}\text{E}$) was 0.75 W m^{-2} in 2006. Recently, Zhuang et al. (2013) showed that the annual mean BC DRF over eastern China ($20^{\circ}\text{--}50^{\circ}\text{N}$, $100^{\circ}\text{--}130^{\circ}\text{E}$) was 0.81 W m^{-2} at the TOA in year 2006, with the strongest TOA BC DRF of 6.0 W m^{-2} over the Sichuan Basin. With respect to global modeling studies, Chung and Seinfeld (2005) showed that the year 2000 TOA BC DRF was the highest ($5\text{--}6 \text{ W m}^{-2}$) in eastern China by using the Goddard Institute for Space Studies General Circulation Model II-prime (GISS GCM II'). Bond et al. (2013) adjusted the absorption optical depth (AAOD) in the median AeroCom model (Aerosol Comparisons between Observations and Models) to be consistent with the AERONET retrieval, and found that the highest TOA DRF of BC of about 4 W m^{-2} was located over eastern China in year 2000. Compared to the long-lived greenhouse gas CO_2 , BC has a much shorter lifetime of days, and therefore BC reduction offers an opportunity to mitigate near-term climate change and to improve air quality simultaneously (Ramanathan and Carmichael, 2008; Shindell et al., 2012; Smith et al., 2013). It is thus important to understand the source attribution of BC in China.

Measurements have been used to attribute sources of BC. Observational studies have analyzed possible sources of BC at several urban sites in China (Li et al., 2005; Tao et al., 2009; Chen et al., 2013; Zhuang et al., 2014; Zhang et al., 2015). Tao et al. (2009) found that the major sources of BC in Guangzhou were industry-coal and vehicle emissions in the winter of 2007, by analyzing the correlations between observed concentrations of BC with those of SO_2 , NO_2 , and NO . Zhuang et al. (2014) suggested that the emissions of BC in Nanjing were mainly from the combustion of biofuel, industry-coal, and vehicle-gasoline, considering the high correlation coefficients (exceeding 0.7 in most seasons in 2012) between observed concentrations of BC and CO. Zhang et al. (2015) found that fossil and biomass burning emissions accounted for about 75% and 25% of BC in four Chinese cities (Beijing, Shanghai, Guangzhou, and Xi'an) during an extreme haze episode in January of 2013, by analyzing the accelerator mass spectrometry measurements of the radiocarbon isotope (^{14}C), since radiocarbon measurements provide a powerful tool for determining fossil and non-fossil sources of carbonaceous aerosols. Such observational studies, however, were usually limited to a particular time period or location or could not provide quantitative estimates.

Regional and global models have been used to quantify the region-based or sector-based contributions to air quality (e.g., Park

et al., 2003; Saikawa et al., 2009; Jeong et al., 2011; M. Huang et al., 2012; Kulkarni et al., 2014) or radiative forcing (e.g., Koch et al., 2007; Shindell et al., 2008; Unger et al., 2008; Anenberg et al., 2011; Streets et al., 2013). By performing sensitivity simulations with the nested version of the GEOS-Chem model, Jeong et al. (2011) reported that anthropogenic emissions in Korea and China contributed 78% and 20%, respectively, to BC concentrations in Korea during March 2006 to February 2007. M. Huang et al. (2012) estimated region contributions to BC concentrations in North America (NA) in summer of 2008 using the Sulfur Transport and Deposition Model (STEM), and found that over 80% of surface BC concentrations in NA were from domestic emissions except in the northwestern America. Because of the long-range transport, 30–80% of column BC concentrations in northwestern America were from non-NA emissions. Kulkarni et al. (2014) reported, on the basis of the simulation with the STEM model, that residential and transport emissions were the most important sectors that contributed to mean BC concentrations in Central Asia during April 2008 to July 2009 (each contributed about 30% to BC concentrations), followed by emissions from industry (contributed about 20% to BC concentrations). Streets et al. (2013), by using the Goddard Institute for Space Studies (GISS)-E2 chemistry-climate model and recent emission inventories, examined the contributions from the major emission sectors in China and India to radiative forcing. They found that the DRF due to all aerosols and O_3 from residential combustion in China reached $1.5\text{--}2 \text{ W m}^{-2}$ over most regions in China. No studies, to our knowledge, have examined sector and region contributions to concentration and DRF of BC in China.

The goal of this study is to quantify the contributions from the major emission sectors in China and non-China emissions to concentration and DRF of BC in China, by using the nested-grid version of the global chemical transport model (GEOS-Chem) and the anthropogenic emission inventory for year 2010 designed for the Task Force on Hemispheric Transport of Air Pollution project (HTAP; <http://www.htap.org/>). Model description and numerical experiments are presented in Section 2. Section 3 shows simulated surface-layer BC concentrations, simulated absorption aerosol optical depth (AAOD) of BC, and model evaluation. Sector and region contributions to BC concentration and DRF in China are presented in Sections 4 and 5, respectively.

2. Model description and numerical experiments

2.1. GEOS-Chem model

We simulate BC concentrations by using the one-way nested-grid GEOS-Chem model (version 9-01-03; <http://acmg.seas.harvard.edu/geos/>) driven by the assimilated GEOS-5 meteorological fields from the Goddard Earth Observing System (GEOS) of the NASA Global Modeling and Assimilation Office (GMAO). The version of the model used here has a horizontal resolution of 0.5° latitude by 0.667° longitude for Asia ($11^{\circ}\text{S}\text{--}55^{\circ}\text{N}$, $70^{\circ}\text{--}150^{\circ}\text{E}$) and 47 vertical layers up to 0.01 hPa. Tracer concentrations at the lateral boundaries are provided by a global GEOS-Chem simulation with horizontal resolution of 4° latitude by 5° longitude (Chen et al., 2009).

The simulation of BC in the GEOS-Chem model was described by Park et al. (2003). BC is represented in the model by two tracers of hydrophobic BC and hydrophilic BC. It is assumed that 80% of freshly emitted BC is hydrophobic and becomes hydrophilic with an e-folding time of 1.15 days (Cooke et al., 1999; Park et al., 2005). The wet deposition scheme of BC in GEOS-Chem was originally described by Liu et al. (2001), including scavenging in convective updrafts, as well as in-cloud (only for hydrophilic BC) and below-cloud scavenging (for both hydrophilic and hydrophobic BC) from

convective and large-scale precipitation. We also include in the present study an improved scheme of BC scavenging by cold clouds and snow following Wang et al. (2011). Dry deposition of aerosols uses the resistance-in-series scheme of Wesely (1989), which is dependent on local surface type and meteorological conditions.

The Rapid Radiative Transfer Model for GCMs (RRTMG) has been coupled online with the GEOS-Chem model as described by Heald et al. (2014). The RRTMG solves the radiative transfer equation in 14 shortwave bands and 16 longwave bands that cover from 230 nm through 56 μm . We calculate instantaneous shortwave and longwave radiative fluxes every 3 h. The DRF of BC is calculated by calling RRTMG twice with and without the presence of BC. The optical properties (extinction coefficient, single scattering albedo, asymmetry factor) of BC are calculated by using the Mie Theory, assuming that BC has a log-normal size distribution with a geometric mean radius of 0.02 μm and a geometric standard deviation of 1.6. We assume that dry BC particles are spherical with a refractive index of 1.75–0.44i at 550 nm and a density of 1 g cm⁻³, following Q. Wang et al. (2014). The DRF of BC is calculated by calling RRTMG twice with and without the presence of BC. It should be noted that the difference in radiative flux with and without BC is sometimes referred to as BC direct radiative effect, but it is about the same as BC DRF because anthropogenic emissions account for more than 99% of BC emissions in China (Lu et al., 2011).

2.2. BC emissions

The global anthropogenic emissions of BC are from Bond et al. (2007), as implemented into the GEOS-Chem by Leibensperger et al. (2012). The global biomass burning emissions of BC are taken from the Global Fire Emissions Database version 3 (GFEDv3) inventory (van der Werf et al., 2010). Anthropogenic emissions of BC in the nested domain (70–150°E, 10°S–55°N) are overwritten by the HTAP anthropogenic emissions for year 2010 (Janssens-Maenhout et al., 2015; http://edgar.jrc.ec.europa.eu/htap_v2/index.php?SECURE=123). The HTAP emission inventory does not have emissions from biomass burning; biomass burning emissions of BC in China are taken from Lu et al. (2011). The total biomass burning emission from GFEDv3 over China is about 15 Gg C for 2010, which is much smaller than the value of 109 Gg C (Table 1) from Lu et al. (2011). T. Fu et al. (2012) also reported that biomass burning emissions retrieved from satellite burnt area observations (Song et al., 2010; van der Werf et al., 2006, 2010) largely underestimated the seasonal agriculture waste burning in China. Fig. 1 shows the horizontal distribution of the anthropogenic emissions of BC and Table 1 summarizes the emissions of BC in China from five major sectors (energy, industry, residential, transportation, and biomass burning) on an annual basis. The annual total BC emission is 1840 Gg C in China, in which emissions from residential, industry, transportation, biomass burning, and energy sectors account for 48.5%, 29.9%, 14.7%, 5.9%, and 1.0%, respectively. The emissions of BC from all sectors have monthly values available. Emissions from

aircraft and shipping are small and hence not considered in our study.

We also summarize in Table 1 the recent estimates of BC emissions in China from the literature. The annual BC emission and contributions from individual sectors in the HATP inventory are comparable to those in other inventories. The HTAP emissions used in our simulation thus well represent the current understanding of BC emissions from each emission sector in China.

2.3. Numerical experiments

To identify the sector and region contributions to concentration and DRF of BC in China, we perform the following GEOS-Chem simulations:

- (1) CTRL: The control simulation with global BC emissions from all sectors;
- (2) no_IND: The same as the CTRL simulation except that BC emissions from industry sector in China are set to zero.
- (3) no_ENG: The same as the CTRL simulation except that BC emissions from energy sector in China are set to zero.
- (4) no_RES: The same as the CTRL simulation except that BC emissions from residential sector in China are set to zero.
- (5) no_TRAS: The same as the CTRL simulation except that BC emissions from transportation sector in China are set to zero.
- (6) no_BB: The same as the CTRL simulation except that BC emissions from biomass burning in China are set to zero;
- (7) no_China: The same as the CTRL simulation except that BC emissions from all sectors in China are set to zero.

The contributions to BC from each Chinese sector of industry, energy, residential, transportation, and biomass burning can be quantified by (CTRL – no_IND), (CTRL – no_ENG), (CTRL – no_RES), (CTRL – no_TRAS), and (CTRL – no_BB), respectively. The results from no_China simulations represent the impacts of non-China BC emissions. Then sector and region contributions to BC in China are obtained by assuming that the BC concentrations simulated in the CTRL simulation are the sum of the contributions from the five domestic sectors and non-China emissions. All simulations are integrated for the period of 1 January to 31 December of year 2010 after a 3-month spin up of the model.

3. Simulated BC and model evaluation

3.1. Simulated surface-layer concentrations of BC

Fig. 2 shows simulated seasonal mean surface-layer concentrations of BC in the CTRL simulation for 2010. The regions with high BC concentrations are consistent with the areas with high BC emissions (Fig. 1). Simulated BC concentrations are the highest in December–January–February (DJF), with concentrations exceeding 9 $\mu\text{g m}^{-3}$ in the North China Plain, the Sichuan Basin, and central

Table 1

Summary of annual BC emissions in China (Unit: Gg C yr⁻¹, 1 Gg = 10⁹ g). Values in the parentheses are the relative contributions to total BC emission from individual emission sectors.

Reference	Year	Energy	Industry	Residential	Transportation	Biomass burning	Total
HTAP (This work)	2010	18 (1.0%)	550 (29.9%)	893 (48.5%)	270 (14.7%)	109 (5.9%) ^a	1840
Lu et al. (2011)	2010	21 (1.1%)	501 (27.1%)	936 (50.6%)	283 (15.3%)	109 (5.9%)	1850
Qin and Xie (2012)	2009	11 (0.6%)	735 (39.1%)	777 (41.3%)	241 (12.8%)	117 (6.2%)	1881
Lu et al. (2011)	2008	19 (1.1%)	510 (28.6%)	888 (49.7%)	259 (14.5%)	110 (6.1%)	1786
Wang et al. (2012)	2007	51 (2.6%)	646 (33.1%)	988 (50.7%)	188 (9.6%)	78 (4.0%)	1951
Zhang et al. (2009)	2006	36 (2.0%)	575 (31.8%)	1002 (55.3%)	198 (10.9%)	N.A.	1811

^a HTAP has no biomass burning emissions of BC in China; biomass burning emissions are taken from Lu et al. (2011).

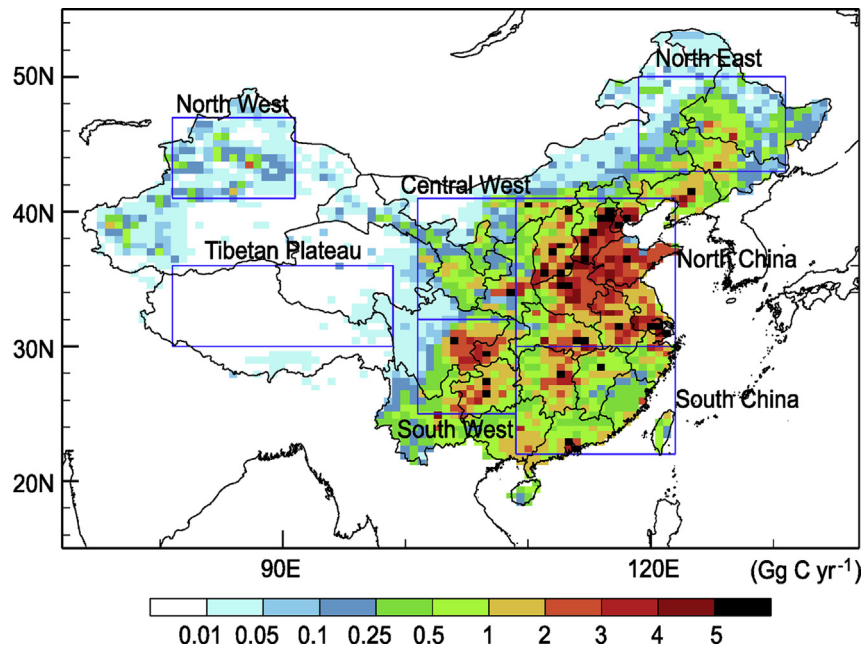


Fig. 1. Horizontal distribution of annual anthropogenic emissions (Gg C yr^{-1}) of BC in China for year 2010. The sub-regions examined in this study are also shown, including two emission regions of North China (109° – 122°E , 30° – 42°N) and South West (101° – 109°E , 25° – 32°N), four low emission regions of South China (109° – 122°E , 22° – 30°N), Central West (101° – 109°E , 32° – 41°N), North East (119° – 131°E , 43° – 50°N), and North West (81° – 91°E , 41° – 47°N), as well as one clean region of Tibet Plateau (81° – 99°E , 30° – 36°N).

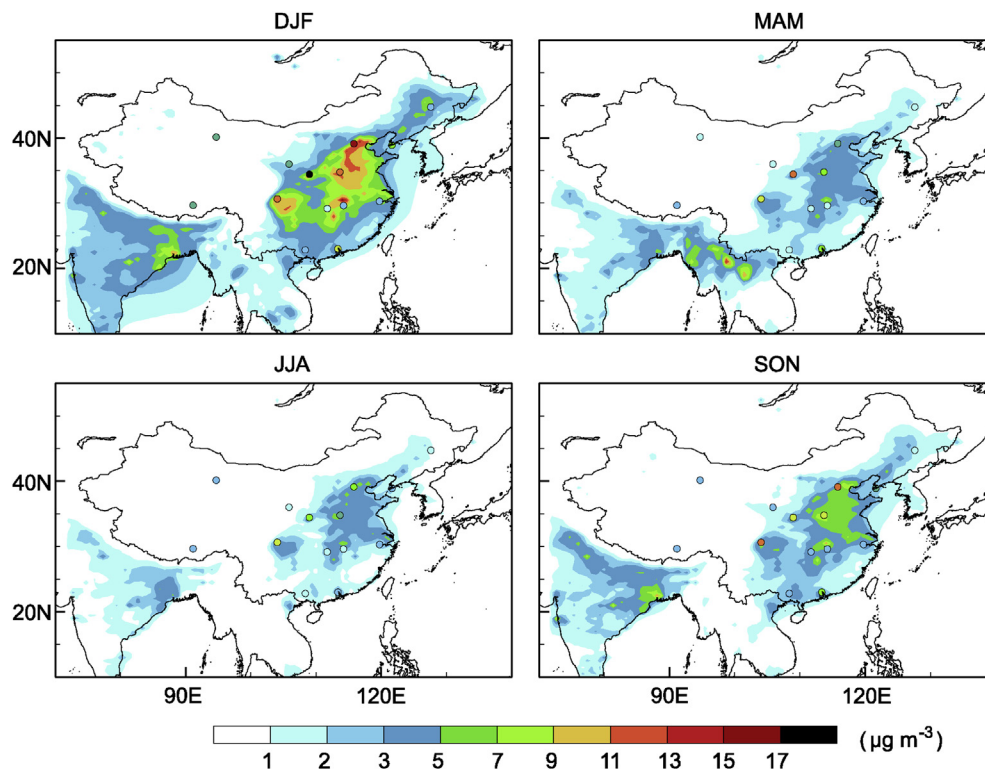


Fig. 2. Simulated seasonal mean surface-layer concentrations ($\mu\text{g m}^{-3}$) of BC in 2010 from the CTRL simulation. Colored circles denote seasonal mean BC concentrations measured at 14 sites of the China Meteorological Administration (CMA) Atmosphere Watch Network (CAWNET) (Zhang et al., 2012).

southern China (e.g., Hubei province). Simulated BC concentrations are the lowest in June–July–August (JJA), with values of 1 – $5 \mu\text{g m}^{-3}$ in a large fraction of eastern China. The lowest BC concentrations in JJA can be attributed to the reduced emissions from domestic heating (Lu et al., 2011) and the enhanced wet deposition during

summer monsoon (Zhang et al., 2010). The magnitudes and distributions of BC simulated in our study are similar to those simulated in T. Fu et al. (2012) and Wang et al. (2013).

We evaluate simulated BC concentrations by using the measurements taken from January 2006 to December 2007 at 14 sites of

the China Meteorological Administration (CMA) Atmosphere Watch Network (CAWNET) (Zhang et al., 2012). The locations of the CAWNET sites are shown in Fig. 2. Fig. 3a compares the simulated versus observed seasonal mean surface-layer concentrations of BC. The simulated BC concentrations have a normalized mean bias (NMB) of -37% (Fig. 3a). The bias in our model results is smaller than the low bias of -56% (at rural and background sites) in T. Fu et al. (2012). The total biomass burning emission of BC in China in our study is 109 Gg C for 2010, very close to the value of 110 Gg C in T. Fu et al. (2012). We use HTAP emissions for year 2010 in this work, while T. Fu et al. (2012) used Intercontinental Chemical Transport Experiment-Phase B (INTEX-B) emissions for year 2006. Although the annual total emission is about the same in these two inventories, BC emissions in the HTAP emission inventory are lower in North China by 3.8% and higher in South China by 3.0% relative to the INTEX-B emissions, (Fig. S1 in the supplementary material), leading to different biases as compared with measurements. Simulated seasonal mean BC concentrations show high correlation ($r = 0.69$) with the observed values (Fig. 3a), indicating that the model can capture the spatial distributions and seasonal variations of BC in China. It should be noted that the observed surface-layer BC concentrations were from years of 2006–2007, while the CTRL

simulation is carried out for year 2010. Our test simulation with both emissions and meteorology of year 2006 shows that the differences in simulated BC concentrations between the CTRL simulation and the test case are small (See Fig. S2 in the supplementary material).

We also evaluate simulated BC concentrations by using additional measurements. Besides the measurements at the 14 CAWNET sites of Zhang et al. (2012), measured annual mean surface-layer BC concentrations (multi-year averages) at additional 30 sites are available from T. Fu et al. (2012), He et al. (2014), and Zhuang et al. (2014). All the measurements are compiled and listed in the supplementary material (Table S1). Fig. 3b shows the scatter plot of observed and simulated annual mean BC concentrations. The simulated BC concentrations have an average bias of -31% as compared with all the BC measurements available, and the correlation coefficient between simulated and observed values is 0.65. The low bias of simulated BC can be attributed to the underestimates of BC concentrations at sites such as Dunhuang, Lhasa, Jinchang, and Xining, which are located in west of 105°E (Fig. 3b).

We compare simulated monthly mean surface BC concentrations with observed values from Zhang et al. (2012) in Fig. 4. The model agrees well with observations at Jinsha, Linan, Longfengshan, Naning, Taiyangshan, and Zhengzhou, although low biases are found at Jinsha and Taiyangshan in winter. Observed BC concentrations were high in winter and low in summer at most sites. This seasonality is well captured by the model except at Dalian, Gucheng, and Panyu. The model underestimates BC concentrations at Xian, Dunhuang, and Lhasa, which may result from the underestimates of local anthropogenic emissions at these western sites.

Note that BC DRF can be influenced by its vertical profile but few aircraft observations of BC vertical profile are available in China. The simulated vertical profiles of BC from the GEOS-Chem model have been evaluated by using datasets from aircraft campaigns for the regions of the Northwest Pacific, North America, and the Arctic in previous studies (Park et al., 2005; Drury et al., 2010; Wang et al., 2011).

3.2. Simulated AAOD of BC

Fig. 5 shows the simulated seasonal mean AAOD of BC from the CTRL simulation. AAOD is calculated as $(1 - \text{SSA}) \times \text{AOD}$, where SSA and AOD are the column single scattering albedo and aerosol optical depth, respectively. Corresponding to the simulated seasonal variations in BC concentrations, AAOD values are the highest in DJF and lowest in JJA. Over eastern China, the maximum AAOD values are about 0.06–0.08 in DJF and 0.03–0.05 in other three seasons. Over the Sichuan Basin, simulated BC AAOD reaches highest values of 0.07–0.09 in DJF.

Since the calculation of DRF of BC is highly sensitive to simulated AAOD, it is essential to evaluate the magnitudes and seasonal variations of AAOD simulated in our model. The observed AAOD in China are available from the Aerosol Robotic Network (AERONET) (Holben et al., 2001). The AERONET sites with retrieved monthly AAOD, the observed BC AAOD values in year 2010, and the averages of BC AAOD over the years with datasets available are listed in Table 2. To compare with model results, BC AAOD at 550 nm are obtained by interpolating measured AAOD at 440 nm and 675 nm, as described in Bond et al. (2013). Note that BC AAOD is estimated by removing AAOD of mineral dust aerosol from the AERONET retrieved AAOD, assuming that the absorption by fine-mode aerosols is primarily from BC while the absorption by larger particles (diameter $> 1 \mu\text{m}$) is principally from dust. Following Bond et al. (2013), dust AAOD is calculated from the retrieved size distribution (diameter $> 1 \mu\text{m}$) provided by the AERONET and a prescribed

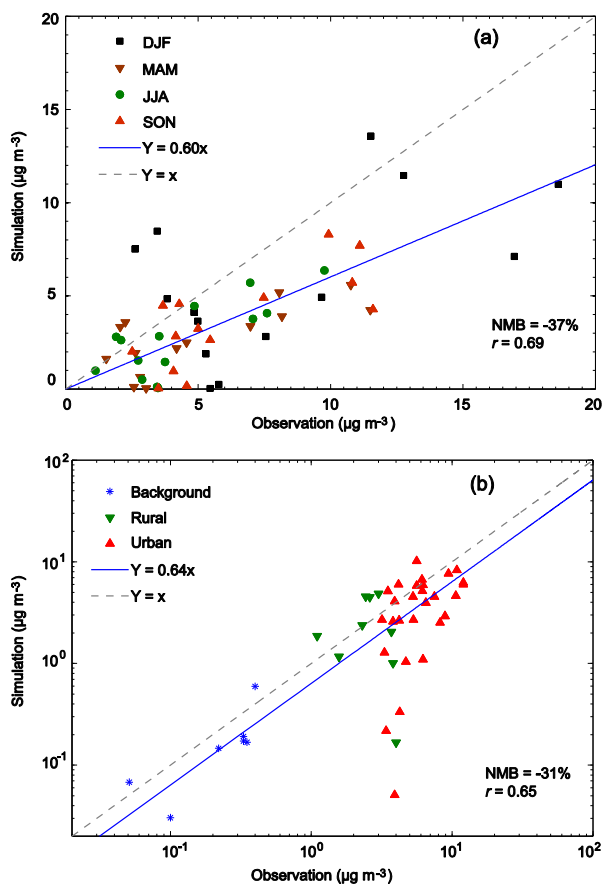


Fig. 3. (a) Comparisons of simulated seasonal mean concentrations of BC with measurements. Simulated values are seasonal averages in 2010 from the CTRL simulation, while the measurements were taken from January 2006 to December 2007 at 14 sites of the China Meteorological Administration (CMA) Atmosphere Watch Network (CAWNET) (Zhang et al., 2012). (b) The same as (a) except that the measurements include annual mean surface-layer BC concentrations (multi-year averages) at additional sites as listed in the supplementary material (Table S1). Also shown is the $y = x$ line (dashed) and linear fit (solid line and equation). Normalized mean bias (NMB) = $100\% \times \sum (M_i - O_i) / \sum O_i$, where M_i and O_i are the simulated concentration and observed value at site i , respectively. r is the correlation coefficient between simulated and measured concentrations.

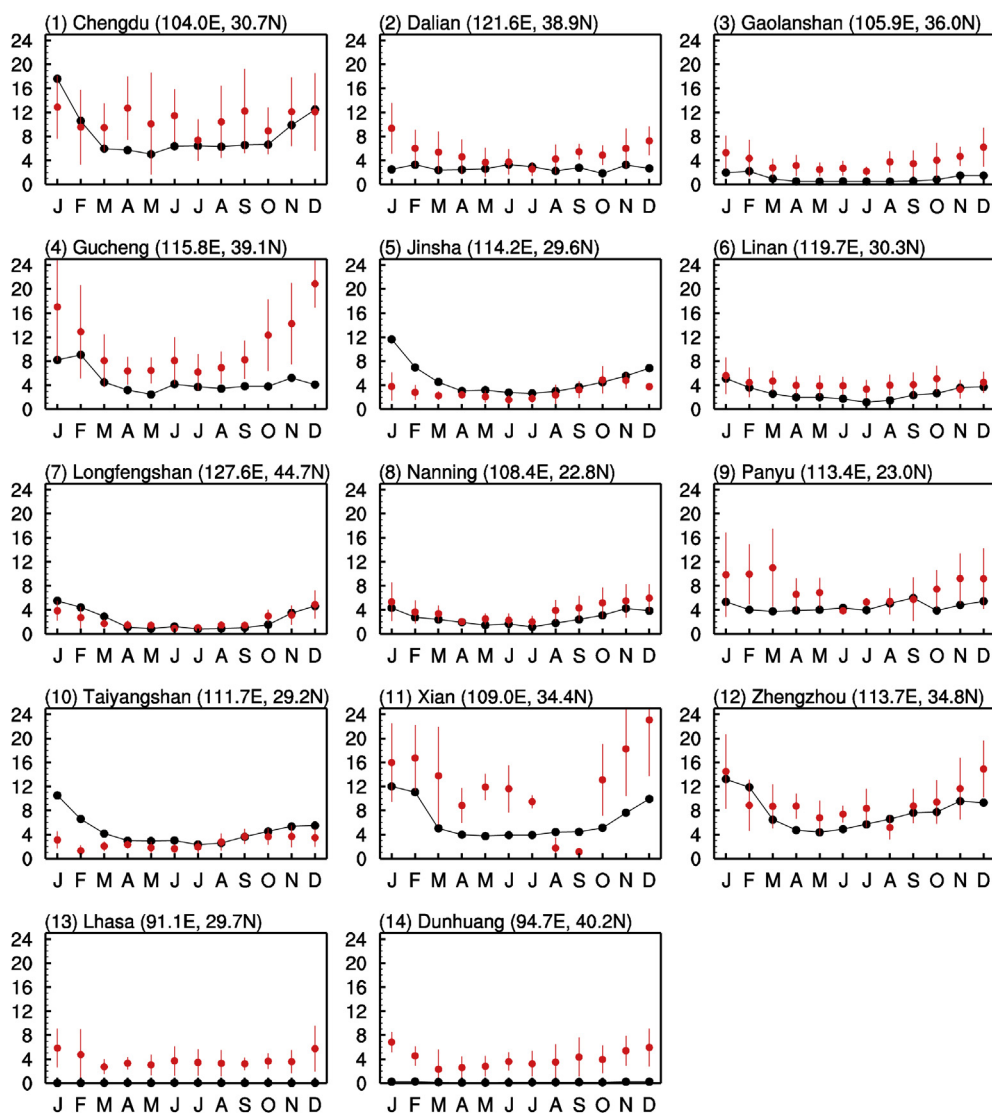


Fig. 4. Comparisons of simulated monthly mean concentrations ($\mu\text{g m}^{-3}$) of BC with measurements. Black dotted lines are simulated values in 2010 from the CTRL simulation, while the red dots are measurements (thin red vertical lines indicate the standard deviations) during January 2006 to December 2007 at 14 sites of the China Meteorological Administration (CMA) Atmosphere Watch Network (CAWNET) (Zhang et al., 2012). (For interpretation of the references to colour in this figure legend, the reader is referred to the web version of this article.)

refractive index of $1.55 + 0.0015i$.

Compared to AERONET measurements at year 2010, simulated BC AAOD values have low biases at all the AERONET sites, with the low biases exceeding 50% at 4 sites (SACOL, Polytechnic U., Hok Tsui, and Chen-Kung U.) (Table 2). We also compare in Table 2 the simulated BC AAOD with the averages of the AERONET measurements over the years with datasets available. Compared to the multi-year averages of the measured AAOD at the 10 sites, our simulated BC AAOD show normalized mean bias (NMB) of -47% , which is higher than the NMB reported by Q. Wang et al. (2014). Q. Wang et al. (2014) showed that the year 2009 BC AAOD simulated in the GEOS-Chem model had an NMB of -32% , as the modeled BC AAOD values were compared to the multi-year averages of derived BC AAOD at the global AERONET sites. We attribute the large low biases in simulated BC AAOD to both the underestimation of BC concentrations in China and the large uncertainties associated with the derived AERONET BC AAOD. Because of the contributions from organic carbon and fine dust to fine-mode AAOD, the derived BC AAOD is likely biased high and the subsequent uncertainty on fine-

mode AAOD can be as large as 40–50% (Bond et al., 2013).

Fig. 6 compares the derived monthly mean BC AAOD with the GEOS-Chem simulations at 10 AERONET sites. At Beijing and the two adjacent sites (Xianghe and Xinglong), the model captures fairly well the declining trend of observed BC AAOD from winter to spring, although simulated AAOD values show low biases in Beijing in spring and in those two adjacent sites in spring and winter. The retrieved BC AAOD from AERONET sites are likely overestimated over North China in spring due to the high concentrations of mineral dust aerosol in this season (Zheng et al., 2005). The model reproduces the observed BC AAOD at Beijing and Xianghe in July and August, but does not capture the peak AAOD values of 0.08–0.10 in June when the harvest practice is active. Several studies (e.g., Li et al., 2008, 2010; X. Huang et al., 2012) have reported that crop residual burning (wheat straw) is a significant source of carbonaceous aerosols in June in North China Plain. Emissions from crop residual burning might have been underestimated in the emission inventory we used. At Taihu, Hefei, and Shouxian (located in Yangtze River Delta and its adjacent regions),

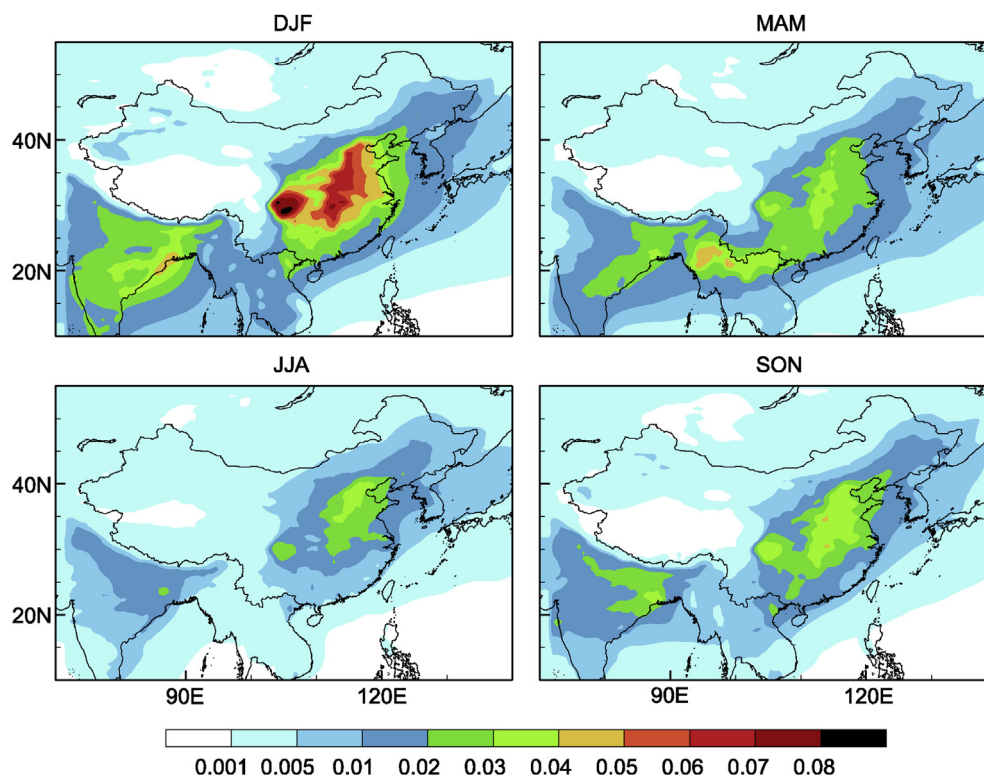


Fig. 5. Simulated seasonal mean BC absorption aerosol optical depth (AAOD) at 550 nm in China from the CTRL simulation.

Table 2

Observed and simulated annual mean BC absorption aerosol optical depth (AAOD) at 10 AERONET sites in China.

Site	Region	Lat. (°N)	Long. (°E)	Elev.(m)	Year	BC AAOD		
						Year 2010 Obs. ^a	Multi-year Obs. ^b	Model ^c
Beijing	Urban	39.98	116.38	92.0	2005–2014	0.060	0.061	0.034
Xianghe	Rural	39.75	116.96	36.0	2005–2012	0.055	0.060	0.039
Xinglong	Rural	40.40	117.58	970.0	2006–2012	0.040	0.033	0.030
Taihu	Rural	31.42	120.22	20.0	2005–2012	0.033	0.054	0.025
Hefei	Urban	31.91	117.16	36.0	2005–2008	N.A.	0.050	0.032
Shouxian	Rural	32.56	116.78	22.7	2008	N.A.	0.039	0.036
SACOL ^d	Rural	35.95	104.14	1965.8	2006–2012	0.029	0.032	0.007
Chen-Kung U. ^e	Urban	23.00	120.22	50.0	2007–2010	0.016	0.016	0.006
Hok Tsui ^f	Rural	22.21	114.26	80.0	2007–2010	0.054	0.041	0.011
Polytechnic U. ^g	Urban	22.30	114.18	30.0	2005–2014	0.063	0.053	0.011

^a Derived AERONET BC AAOD for 2010.

^b Multi-year averages of the derived AERONET BC AAOD over years with datasets available.

^c Simulated BC AAOD from the CTRL simulation for 2010.

^d SACOL: Semi-Arid Climate and Environment Observatory of Lanzhou University.

^e Chen-Kung U. site is located in Chen-Kung University, Tainan City, Taiwan.

^f Observations at Hok Tsui were carried out only from March to June in 2010.

^g Polytechnic U. is located in Hong Kong Polytechnic University, Hong Kong.

simulated BC AAOD values agree well with the observations in all seasons. In northwestern China, the simulated BC AAOD is significantly underestimated at SACOL. The large low bias at this site can be attributed to the large uncertainties in the derived BC AAOD, due to the observed high concentrations of mineral aerosol in northwestern China (Zhang et al., 2012). In southeast coastal China, both observed and simulated BC AAOD show high peaks in March at the sites of Hok Tsui, Polytechnic U., and Chen-Kung U., but the model tends to underestimate BC AAOD at Hok Tsui and Polytechnic University throughout the year possibly because of the underestimates of local anthropogenic emissions and biomass burning emissions in Southeast Asia. The high AAOD at these sites in March is influenced by the long-range transport of biomass

burning emissions from Southeast Asia (J. Fu et al., 2012; Huang et al., 2013; Lin et al., 2014).

4. Sector and region contributions to BC concentrations

Fig. 7 shows the simulated contributions to surface-layer BC concentrations from five domestic emission sectors (residential, industry, energy, transportation, and biomass burning) and non-China emissions, based on the six sensitivity simulations described in Section 2.4. In the North China Plain and the Sichuan Basin (the densely populated regions), residential sector is the largest contributor to surface BC concentrations. Residential emissions contribute to surface-layer BC concentrations by 5–7 $\mu\text{g m}^{-3}$

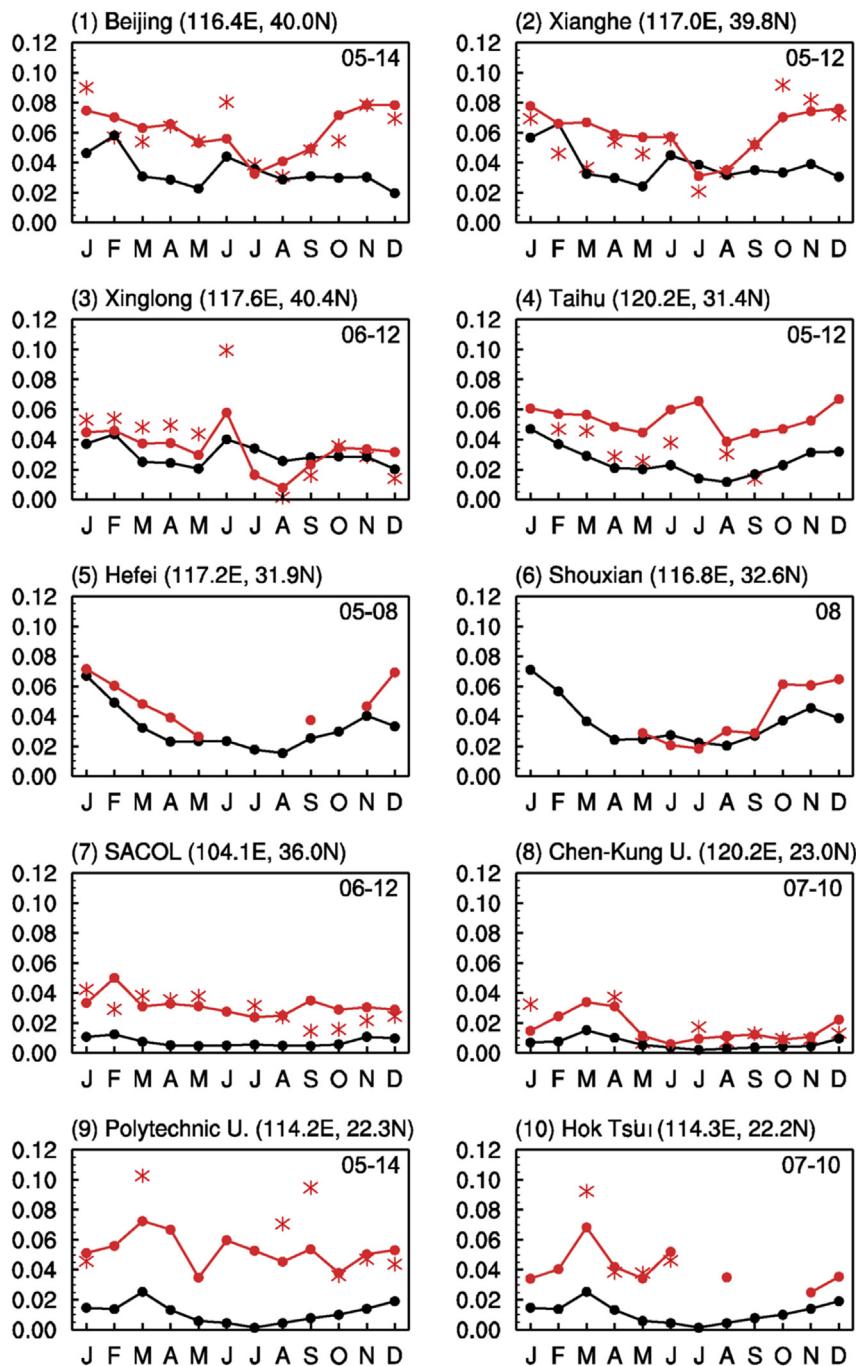


Fig. 6. Comparisons of monthly mean BC AAOD from AERONET retrievals with those from the CTRL simulation at the ten AERONET sites. Black lines are simulated BC AAOD for 2010, the asterisks are the AERONET BC AAOD in year 2010, and red dotted lines are multi-year averages of the AERONET BC AAOD over years with datasets available (marked on top right corner of each panel). (For interpretation of the references to colour in this figure legend, the reader is referred to the web version of this article.)

in DJF and by $1\text{--}3\ \mu\text{g m}^{-3}$ in JJA, reflecting the strong emissions from winter heating (Lu et al., 2011) and enhanced wet deposition during summer monsoon (Zhang et al., 2010). The contribution from industry sector is the second largest and shows relatively small seasonal variations; the emissions from industry sector lead to BC concentrations of $1\text{--}3\ \mu\text{g m}^{-3}$ in the North China Plain and the Sichuan Basin. The contribution from transportation sector is the third largest. The maximum impacts of emissions from transportation are located in the North China Plain, which are in the range of $1\text{--}2\ \mu\text{g m}^{-3}$ in DJF and of $0.5\text{--}1\ \mu\text{g m}^{-3}$ in JJA. The contribution from energy sector is relatively small, contributing to

surface-layer BC concentrations by less than $0.1\ \mu\text{g m}^{-3}$ across China. Biomass burning emissions contribute less than $0.5\ \mu\text{g m}^{-3}$ across China, except in September–October–November (SON). The highest concentrations from biomass burning are $0.5\text{--}1\ \mu\text{g m}^{-3}$ in the North China Plain in SON, because of the large agricultural waste burning (Cao et al., 2006). Compared with domestic emissions, non-China emissions contribute relatively small to surface-layer concentrations of BC in China. The maximum contributions from non-China sources are simulated to be $0.1\text{--}0.5\ \mu\text{g m}^{-3}$ in southwestern China in March–April–May (MAM) and DJF (Fig. 7), owing to the high biomass burning emissions in Southeast Asia that

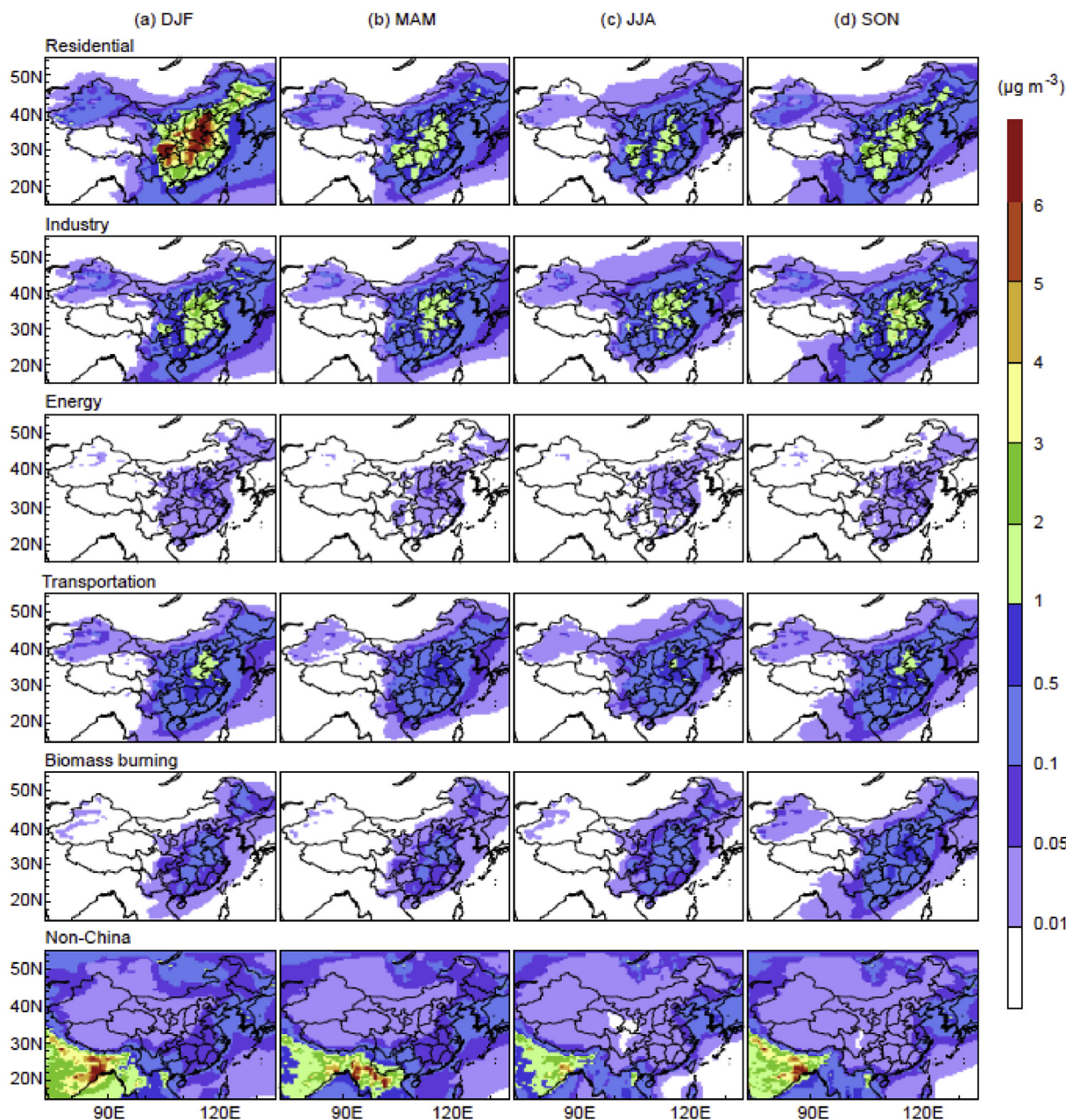


Fig. 7. Simulated contributions to surface-layer concentrations of BC ($\mu\text{g m}^{-3}$) from five domestic emission sectors in China (residential, industry, energy, transportation, and biomass burning) and non-China emissions for year 2010.

can be transported to the adjacent regions in the boundary layer (Jian and Fu, 2014).

Fig. 8a shows the simulated contributions to surface-layer BC concentrations from five domestic emission sectors and non-China emissions that are averaged over the sub-regions, including two emission regions of North China (NC, 109° – 122°E , 30° – 42°N) and South West (SW, 101° – 109°E , 25° – 32°N), four low emission regions of South China (SC, 109° – 122°E , 22° – 30°N), Central West (CW, 101° – 109°E , 32° – 41°N), North East (NE, 119° – 131°E , 43° – 50°N), and North West (NW, 81° – 91°E , 41° – 47°N), as well as one clean region of Tibet Plateau (TP, 81° – 99°E , 30° – 36°N). The domains of these sub-regions are shown in Fig. 1. In DJF, residential emissions are dominant in both high emission regions (NC and SW) and low emission regions (SC, CW, and NE), which contribute to surface-layer BC concentrations in these sub-regions by about

60–70%. In MAM, JJA, and SON, residential and industry emissions are the two major sources that contribute to surface BC concentrations in all regions except in NW and TP, and the contributions are comparable between industry (23–46%) and residential (24–58%) emissions. The contribution from transportation is about 10–15% throughout the year in all sub-regions except for TP. On an annual mean basis, the contributions from transportation emissions are the highest in SC (15%), NC (14%), and NE (14%). Over TP, transportation sector contributes 6–9% to surface BC concentrations. The contributions from domestic biomass burning emissions are the largest in SON and are estimated to be 9%, 7%, 12%, 7%, 11%, and 9%, respectively, in NC, SW, SC, CW, NE, and NW. The contributions from the non-China emissions are the highest over TP, which are calculated to be 71%, 76%, 68%, and 64% (Fig. 8a), in DJF, MAM, JJA, and SON, respectively. Our results over TP are consistent

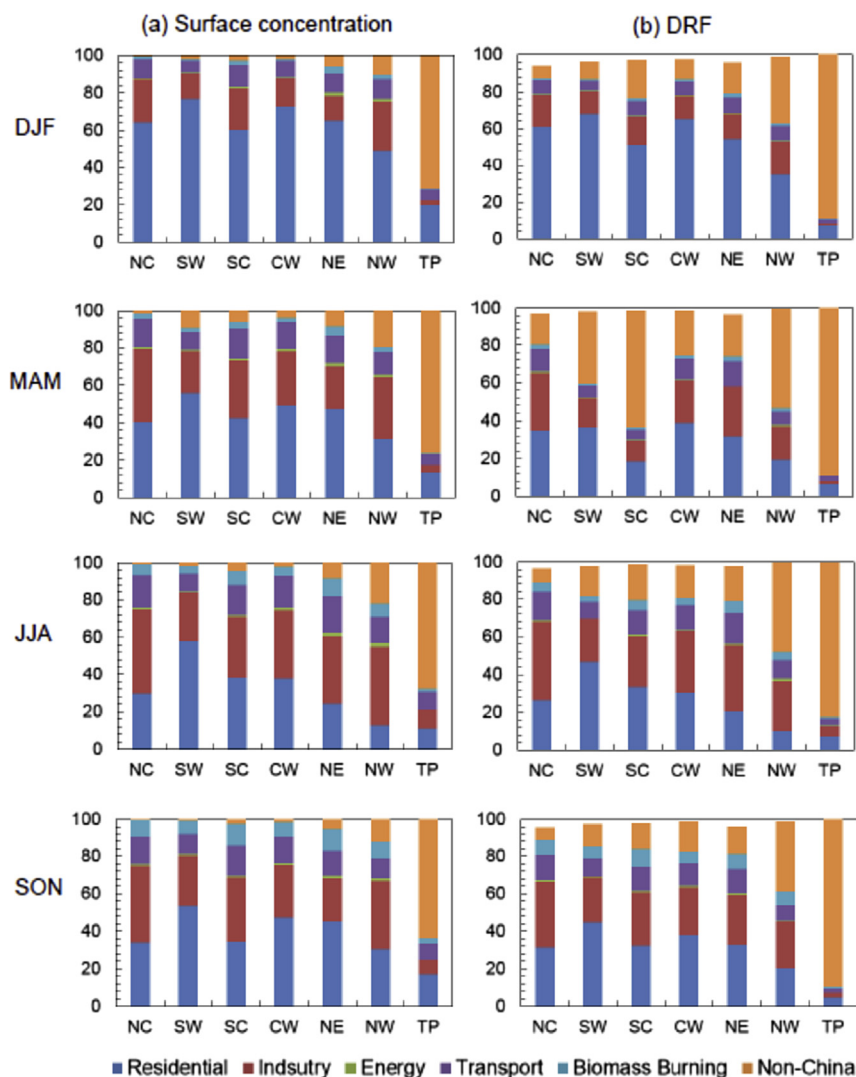


Fig. 8. Relative contributions (%) to (a) surface-layer BC concentration and (b) all-sky DRF of BC at the TOA from five domestic emission sectors in China (residential, industry, energy, transportation, and biomass burning) and non-China emissions over the seven sub-regions as defined in Fig. 1.

with those from previous studies. By using a back-trajectory approach, Lu et al. (2012) reported that emissions in China accounted for 9% (34%) of BC transported to the TP in winter (summer).

Because the vertical distribution of BC is very important for the calculation of BC DRF, we show in Fig. 9a the simulated vertical profiles of BC mass concentration from both the CTRL and no-China simulations. The contributions from non-China emissions to vertical profiles of BC are shown in Fig. 9b ($\text{no_China} \times 100\%/\text{CTRL}$). The non-China emissions influence vertical profiles of BC from the surface to about 6 km altitude in the regions of SC, SW, NE, and NW, and influence the vertical profile of BC throughout the troposphere in TP (Fig. 9a). The large impacts on profiles of BC in SC and SW in spring result from the transport of biomass burning emissions from Southeast Asia. On a seasonal mean basis, the non-China emissions contribute to BC concentrations at 5 km altitude by 20–50% in NC, 20–80% in SC and SW, 40–75% in CW, about 40% in NE, and >80% in NW and TP, and the percentage contributions generally increase with altitudes. Previous studies have shown that the direct radiative forcing efficiency of BC (radiative forcing exerted per gram of BC) increases with altitude due to the radiative interactions with clouds, other aerosols, and ambient air (Samset and Myhre, 2011,

2015; Samset et al., 2013), and BC above 5 km accounts for $41 \pm 14\%$ of the global BC DRF (Samset et al., 2013). Our results highlight the impacts of non-China emissions on vertical profiles and hence DRF of BC in China, even over the regions with high domestic emissions (e.g., SW).

5. Sector and region contributions to direct radiative forcing of BC

Fig. 10 shows the simulated seasonal mean all-sky DRF of BC at the top of the atmosphere (TOA) for 2010. The strongest BC DRF is simulated to occur in DJF, with high forcing values of $8\text{--}11 \text{ W m}^{-2}$ in the Sichuan Basin, $6\text{--}8 \text{ W m}^{-2}$ over the North China Plain and central southern China (e.g., Hubei and Hunan provinces). In MAM, the strongest BC DRF of $4\text{--}6 \text{ W m}^{-2}$ is simulated in southern China. The locations of maximum DRF in JJA and SON are about the same as those in DJF, and the maximum forcing values of $5\text{--}6 \text{ W m}^{-2}$ and $4\text{--}5 \text{ W m}^{-2}$ are simulated in JJA and SON, respectively.

The comparisons of our simulated BC DRF in China with the values reported in previous studies are shown in Table 3. On an annual mean basis, our simulated BC DRF averaged over all of China is 1.22 W m^{-2} and the regional maximum values reach about

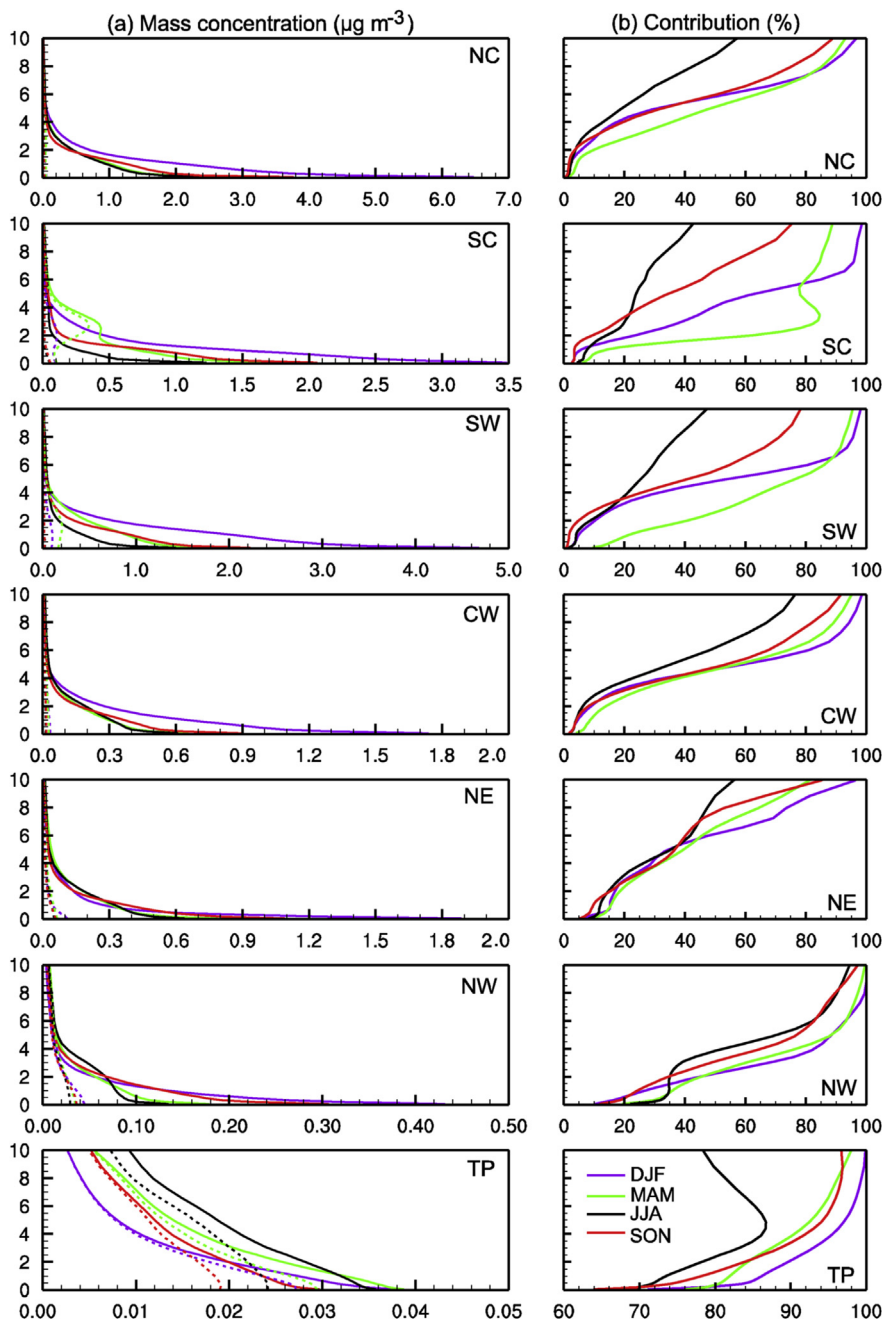


Fig. 9. (a) Simulated vertical profiles of BC mass concentration ($\mu\text{g m}^{-3}$) from the CTRL simulation (solid lines) and the no-China simulation (with non-China emissions alone, dashed lines) that are averaged over the seven sub-regions defined in Fig. 1. (b) The contributions of non-China emissions to vertical BC mass concentrations ($\text{no_China} \times 100\% / \text{CTRL}$) over the seven sub-regions. The unit of vertical axis is km, and the four seasons of DJF, MAM, JJA, and SON are represented by purple, green, black, and red colors, respectively. (For interpretation of the references to colour in this figure legend, the reader is referred to the web version of this article.)

$5\text{--}6 \text{ W m}^{-2}$, which are at the high end of the values obtained in previous modeling studies. The annual BC emission over China is the highest in our work (1840 Gg) among the studies listed in Table 3, but the simulated BC DRF also depends on other factors such as concentration, vertical profile, optical properties (associated with refractive index, mixing state, and particle size of BC), as well as local conditions of surface albedo and clouds (Liao and Seinfeld, 1998). Compared to the global annual mean DRF values of BC (0.4 W m^{-2}), tropospheric ozone (0.4 W m^{-2}), and carbon dioxide (1.82 W m^{-2}) reported by IPCC (2013), the simulated BC DRF averaged over China (1.22 W m^{-2}) is quite significant.

Fig. 11 shows the simulated contributions to all-sky BC DRF at TOA from five domestic emission sectors and non-China emissions. The spatial distributions of BC DRF mimic those of concentrations (Fig. 7). In DJF, the simulated DRF values from residential sector are below 1.0 W m^{-2} in most areas of western China (west of 105° E), $3\text{--}5 \text{ W m}^{-2}$ in eastern China (e.g., Hubei and Henan provinces), and even reach $6\text{--}7 \text{ W m}^{-2}$ in the Sichuan Basin. In JJA, the DRF from residential sector decreases to its minimum of the year of about $1\text{--}2 \text{ W m}^{-2}$ over the North China Plain and Sichuan Basin. The DRF from industry sector shows relatively small seasonal variations, with the forcing values of about $0.5\text{--}2 \text{ W m}^{-2}$ in the North China

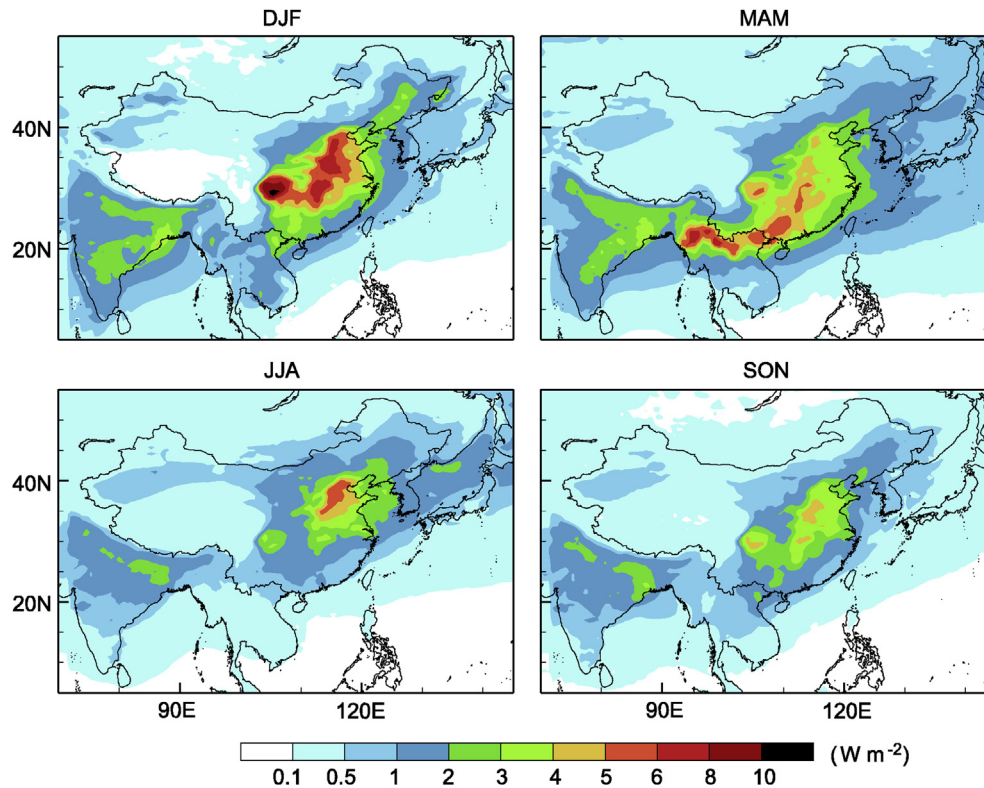


Fig. 10. Simulated seasonal mean all-sky direct radiative forcing (DRF) of BC (W m^{-2}) at the top of the atmosphere (TOA) in year 2010.

Table 3

Comparison of the simulated annual mean all-sky BC DRF at the top of the atmosphere in China in this work with the values reported in previous studies.

Reference	Model	Year	BC emission in China Tg yr^{-1}	Extinction coefficient at $550 \text{ nm } \mu\text{m}^2 \text{ g}^{-1}$	Region	DRF (W m^{-2})	
						Annual mean ^a	Maximum value ^b
This study	GEOS-Chem ^c	2010	1840	8.5	All of China ($100^{\circ}\text{--}130^{\circ}\text{E}$, $20^{\circ}\text{--}50^{\circ}\text{N}$)	1.22	5–6
Zhuang et al. (2011)	RegCCMS	2006	1811	10	($100^{\circ}\text{--}130^{\circ}\text{E}$, $25^{\circ}\text{--}45^{\circ}\text{N}$)	1.46	6
Zhuang et al. (2013)	RegCCMS	2006	1811	10	($100^{\circ}\text{--}130^{\circ}\text{E}$, $20^{\circ}\text{--}50^{\circ}\text{N}$)	0.75	6
Q. Wang et al. (2014)	GEOS-Chem ^d	2009	1811	11.3 ^e	($95^{\circ}\text{--}125^{\circ}\text{E}$, $18^{\circ}\text{--}45^{\circ}\text{N}$)	0.81	5–7.5
Chang and Liao (2009)	GISS GCM II'	2000	1600 ^f	12.5		0.58	
X. Wang et al. (2014)	GEOS-Chem ^g	2010	1508	8.2/9.6			4
Chung et al. (2012)	MACR model ^h	2001–2009	1489	N.A.			7
Chung and Seinfeld (2005)	GISS GCM II'	2000	1489	12.5			5–6
Myhre et al. (2009)	Oslo CTM2	2004	1420	13.0			3–4
Bond et al. (2013)	AeroCom Model I ⁱ	2000	1420	8.9			4
Wu et al. (2008)	RegCM3	1993–2003	1005	12.5	($105^{\circ}\text{--}120^{\circ}\text{E}$, $32^{\circ}\text{--}50^{\circ}\text{N}$)	1.10	3

^a Annual mean BC DRF averaged over the region shown in this table.

^b Maximum value means the largest BC DRF found over the domain of China.

^c DRF is calculated online using RRTMG, with BC refractive index of $1.75\text{--}0.44i$ and density of 1 g cm^{-3} .

^d DRF is calculated offline using a radiative transfer model (RTM) of Wang et al. (2008), with BC refractive index of $1.76\text{--}0.47i$ and density of 1 g cm^{-3} .

^e Shown here is mass absorption coefficient (MAC). $\text{MAC} = \text{MEC} \times (1\text{--SSA})$, where MEC and SSA are the mass extinction coefficient and single scattering albedo of BC calculated from the Mie code, respectively.

^f Emissions are summed over ($18^{\circ}\text{--}45^{\circ}\text{N}$, $95^{\circ}\text{--}125^{\circ}\text{E}$).

^g DRF is calculated online using RRTMG, with BC refractive index of $1.95\text{--}0.79i$ and density of 1.8 g cm^{-3} . Emissions are scaled up by 16% compared with emissions of Bond et al. (2007). Extinction coefficient is $8.2 \text{ m}^2 \text{ g}^{-1}$ for fossil fuel BC and $9.6 \text{ m}^2 \text{ g}^{-1}$ for biofuel/biomass burning BC.

^h Monte-Carlo Aerosol Cloud Radiation (MACR) model. DRF is calculated by using observed BC AOD from the AERONET.

ⁱ Aerosol Comparisons between Observations and Models. BC DRF is the median in AeroCom models with simulated AAOD adjusted to be consistent with the AERONET retrieval.

Plain throughout the year. The transportation sector contributes about $0.5\text{--}1 \text{ W m}^{-2}$ to BC DRF in the North China Plain. The contributions from biomass burning and energy sectors are relatively small, with DRF from biomass burning less than 0.5 W m^{-2} and that from energy sector less than 0.05 W m^{-2} across China.

The BC DRF from non-China emissions is largest in south of

Yangtze River basin in China, with high BC DRF values of $1\text{--}5 \text{ W m}^{-2}$ and $0.5\text{--}2 \text{ W m}^{-2}$ in MAM and DJF, respectively. Note that the fractional contributions of non-China emissions to BC DRF are significantly larger than those to surface BC concentration (Fig. 8a and b), because high emissions in Southeast Asia are not only transported to the boundary layer of the adjacent southern

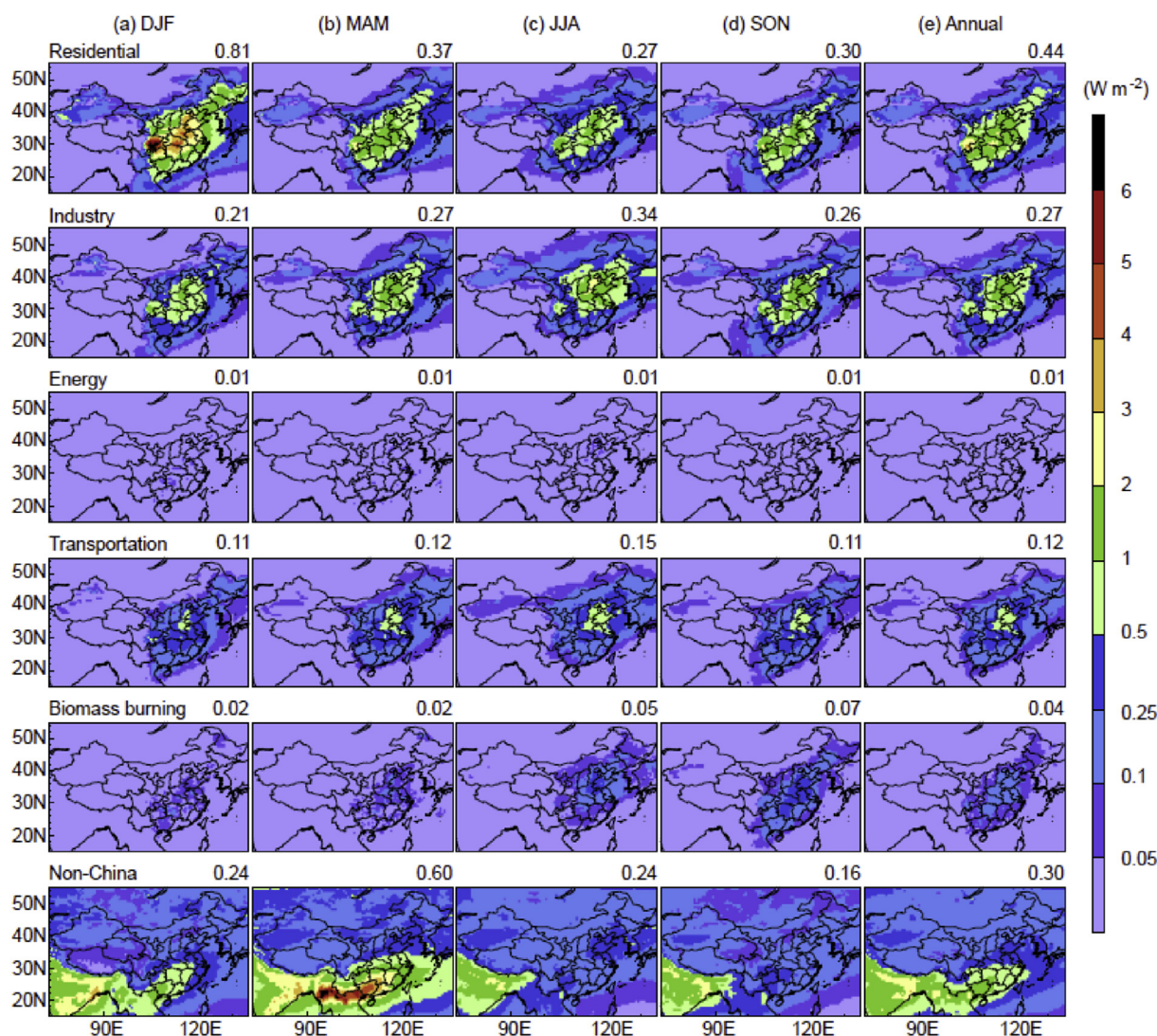


Fig. 11. Simulated contributions to all-sky TOA DRF of BC (W m^{-2}) from five domestic emission sectors in China (residential, industry, energy, transportation, and biomass burning) and non-China emissions for year 2010. The seasonal or annual averages (W m^{-2}) of the BC DRF over China are shown on top right corner of each panel.

China but also lifted to the free troposphere (Bey et al., 2001; Phadnis et al., 2002; Liu et al., 2003; Deng et al., 2008; Jian and Fu, 2014). Studies have shown that vertical injection of seasonal biomass burning emissions (during December–May with a peak in March) in southeast Asia (Jian and Fu, 2014) and convective and large-scale lifting of mixed anthropogenic and biomass burning emissions (Phadnis et al., 2002; Liu et al., 2003) are the two important ways of BC into the free troposphere. Averaged over all of China, contributions from non-China emissions to BC DRF in China are estimated to be 17%, 43%, 21%, and 17%, in DJF, MAM, JJA, and SON, respectively.

On an annual mean basis, BC direct radiative forcings averaged over all of China from five domestic emission sectors of residential, industry, energy, transportation, biomass burning, and non-China emissions are 0.44, 0.27, 0.01, 0.12, 0.04, and 0.30 W m^{-2} , respectively. The domestic and non-China emissions contribute about 75% and 25% to BC DRF in China, respectively.

6. Conclusions

We used a nested-grid version of the global chemical transport

model (GEOS-Chem) coupled with a radiative transfer module (RRTMG) to estimate the contributions from five emission sectors (residential, industry, transportation, energy, biomass burning) in China and emissions from outside of China to concentration and direct radiative forcing of BC in China for year 2010. The HTAP anthropogenic emissions of BC for year 2010 are used in this study. The annual total BC emission in China is 1840 Gg C, in which emissions from residential, industry, transportation, biomass burning, and energy sectors account for 48.5%, 29.9%, 14.7%, 5.9%, and 1.0%, respectively. Comparisons of simulated surface-layer BC concentrations with multi-year averages of measurements at urban, rural, and background sites show that the GEOS-Chem model can capture the spatial distributions and seasonal variations of BC, with a normalized mean bias of -31% and a high correlation coefficient of 0.65.

Simulated surface-layer BC concentrations exceed $9 \mu\text{g m}^{-3}$ in DJF and are about $1\text{--}5 \mu\text{g m}^{-3}$ in the North China Plain and the Sichuan Basin. Residential sector has the largest contribution to surface BC concentrations, by $5\text{--}7 \mu\text{g m}^{-3}$ in DJF and by $1\text{--}3 \mu\text{g m}^{-3}$ in JJA. The contribution from industry sector is the second largest and shows relatively small seasonal variations; the emissions from

industry sector lead to BC concentrations of 1–3 $\mu\text{g m}^{-3}$ in the North China Plain and the Sichuan Basin. The contribution from transportation sector is the third largest, followed by that from biomass burning and energy sectors. The maximum contributions from non-China sources are simulated to be 0.1–0.5 $\mu\text{g m}^{-3}$ in southwestern China in MAM and DJF, owing to the high biomass burning and anthropogenic emissions in Southeast Asia in these seasons. We also find that the non-China emissions have large impacts on vertical profiles of BC over China.

Averaged over all of China, the all-sky DRF of BC at TOA is simulated to be 1.22 W m^{-2} in the CTRL simulation. Sensitivity simulations show that the TOA BC direct radiative forcings from five domestic emission sectors of residential, industry, energy, transportation, biomass burning, and non-China emissions are 0.44, 0.27, 0.01, 0.12, 0.04, and 0.30 W m^{-2} , respectively. The domestic and non-China emissions contribute 75% and 25% to BC DRF in China, respectively. These results have important implications for taking measures to reduce BC emissions to mitigate near-term climate change and to improve air quality simultaneously.

There are some uncertainties in our simulations that can be improved in future studies. First, co-emitted species with BC should be considered to examine sector contributions to radiative forcing. Second, estimates of BC radiative forcing depend on its optical properties and vertical distributions (Bond et al., 2013; Samset et al., 2013), which requires more observational studies to constrain the model uncertainties. Third, the mixing state and aging process of BC should be considered in the simulation of BC radiative forcing. Finally, the consideration of BC–cloud interactions is essential for better understanding the role of BC in climate.

Acknowledgments

This work was supported by the National Basic Research Program of China (973 program, Grant 2014CB441202), the Strategic Priority Research Program of the Chinese Academy of Sciences (Grant No. XDA05100503), and the National Natural Science Foundation of China under grants 41475137 and 41321064. We acknowledge the efforts of the EDGAR team for providing the HTAP emissions and the AERONET team for providing the aerosol datasets used in our study.

Appendix A. Supplementary data

Supplementary data related to this article can be found at <http://dx.doi.org/10.1016/j.atmosenv.2015.06.014>.

References

- Anenberg, S.C., Talgo, K., Arunachalam, S., Dolwick, P., Jang, C., West, J.J., 2011. Impacts of global, regional, and sectoral black carbon emission reductions on surface air quality and human mortality. *Atmos. Chem. Phys.* 11 (14), 7253–7267. <http://dx.doi.org/10.5194/acp-11-7253-2011>.
- Bey, I., Jacob, D.J., Logan, J.A., Yantosca, R.M., 2001. Asian chemical outflow to the Pacific in spring: origins, pathways, and budgets. *J. Geophys. Res.* Atmos. 106 (D19), 23097–23113. <http://dx.doi.org/10.1029/2001JD000806>.
- Bond, T.C., Streets, D.G., Yarber, K.F., Nelson, S.M., Woo, J.-H., Klimont, Z., 2004. A technology-based global inventory of black and organic carbon emissions from combustion. *J. Geophys. Res.* Atmos. 109 (D14), D14203. <http://dx.doi.org/10.1029/2003JD003697>.
- Bond, T.C., Bhardwaj, E., Dong, R., Jogani, R., Jung, S., Roden, C., Trautmann, N.M., 2007. Historical emissions of black and organic carbon aerosol from energy-related combustion, 1850–2000. *Glob. Biogeochem. Cy.* 21 (2), GB2018. <http://dx.doi.org/10.1029/2006GB002840>.
- Bond, T.C., Doherty, S.J., Fahey, D.W., Forster, P.M., Berntsen, T., DeAngelo, B.J., Flanner, M.G., Ghan, S., Kärcher, B., Koch, D., Kinne, S., Kondo, Y., Quinn, P.K., Sarofim, M.C., Schultz, M.G., Schulz, M., Venkataraman, C., Zhang, H., Zhang, S., Bellouin, N., Guttikunda, S.K., Hopke, P.K., Jacobson, M.Z., Kaiser, J.W., Klimont, Z., Lohmann, U., Schwarz, J.P., Shindell, D., Storelvmo, T., Warren, S.G., Zender, C.S., 2013. Bounding the role of black carbon in the climate system: scientific assessment. *J. Geophys. Res.* Atmos. 118 (11), 5380–5552. <http://dx.doi.org/10.1002/jgrd.50171>.
- Cao, G.L., Zhang, X.Y., Zheng, F.C., 2006. Inventory of black carbon and organic carbon emissions from China. *Atmos. Environ.* 40 (34), 6516–6527. <http://dx.doi.org/10.1016/j.atmosenv.2006.05.070>.
- Chang, W.Y., Liao, H., 2009. Anthropogenic direct radiative forcing of tropospheric ozone and aerosols from 1850 to 2000 estimated with IPCC AR5 emissions inventories. *Atmos. Ocean. Sci. Lett.* 2, 201–207.
- Chen, D., Wang, Y., McElroy, M.B., He, K., Yantosca, R.M., Le Sager, P., 2009. Regional CO pollution and export in China simulated by the high-resolution nested-grid GEOS-Chem model. *Atmos. Chem. Phys.* 9 (11), 3825–3839. <http://dx.doi.org/10.5194/acp-9-3825-2009>.
- Chen, H.Z., Wu, D., Liao, B.T., Li, H.Y., Li, F., 2013. Compare of black carbon concentration variation between Dongguan and Maofengshan. *China Environ. Sci.* 33 (4), 605–612. <http://dx.doi.org/10.3969/j.issn.1000-6923.2013.04.005> (in Chinese).
- Chung, S.H., Seinfeld, J.H., 2005. Climate response of direct radiative forcing of anthropogenic black carbon. *J. Geophys. Res.* Atmos. 110 (D11), D11102. <http://dx.doi.org/10.1029/2004JD005441>.
- Chung, C.E., Lee, K., Müller, D., 2012. Effect of internal mixture on black carbon radiative forcing. *Tellus B* 64, 10925. <http://dx.doi.org/10.3402/tellusb.v64i0.10925>.
- Cooke, W.F., Lioussé, C., Cachier, H., Feichter, J., 1999. Construction of a $1^\circ \times 1^\circ$ fossil fuel emission data set for carbonaceous aerosol and implementation and radiative impact in the ECHAM4 model. *J. Geophys. Res.* Atmos. 104 (D18), 22137–22162. <http://dx.doi.org/10.1029/1999JD900187>.
- Deng, X.J., Tie, X.X., Zhou, X.J., Wu, D., Zhong, L.J., Tan, H.B., Li, F., Huang, X.Y., Bi, X.Y., Deng, T., 2008. Effects of Southeast Asia biomass burning on aerosols and ozone concentrations over the Pearl River Delta (PRD) region. *Atmos. Environ.* 42 (36), 8493–8501. <http://dx.doi.org/10.1016/j.atmosenv.2008.08.013>.
- Drury, E., Jacob, D.J., Spurr, R.J.D., Wang, J., Shinozuka, Y., Anderson, B.E., Clarke, A.D., Dibb, J., McNaughton, C., Weber, R., 2010. Synthesis of satellite (MODIS), aircraft (ICARTT), and surface (IMPROVE, EPA-AQS, AERONET) aerosol observations over eastern North America to improve MODIS aerosol retrievals and constrain surface aerosol concentrations and sources. *J. Geophys. Res.* Atmos. 115 (D14) <http://dx.doi.org/10.1029/2009JD012629>.
- Fu, J.S., Hsu, N.C., Gao, Y., Huang, K., Li, C., Lin, N.H., Tsay, S.C., 2012. Evaluating the influences of biomass burning during 2006 BASE-ASIA: a regional chemical transport modeling. *Atmos. Chem. Phys.* 12 (9), 3837–3855. <http://dx.doi.org/10.5194/acp-12-3837-2012>.
- Fu, T.M., Cao, J.J., Zhang, X.Y., Lee, S.C., Zhang, Q., Han, Y.M., Qu, W.J., Han, Z., Zhang, R., Wang, Y.X., Chen, D., Henze, D.K., 2012. Carbonaceous aerosols in China: top-down constraints on primary sources and estimation of secondary contribution. *Atmos. Chem. Phys.* 12 (5), 2725–2746. <http://dx.doi.org/10.5194/acp-12-2725-2012>.
- He, C., Li, Q.B., Liou, K.N., Zhang, J., Qi, L., Mao, Y., Gao, M., Lu, Z., Streets, D.G., Zhang, Q., Sarin, M.M., Ram, K., 2014. A global 3-D CTM evaluation of black carbon in the Tibetan Plateau. *Atmos. Chem. Phys.* 14 (13), 7091–7112. <http://dx.doi.org/10.5194/acp-14-7091-2014>.
- Heald, C.L., Ridley, D.A., Kroll, J.H., Barrett, S.R.H., Cady-Pereira, K.E., Alvarado, M.J., Holmes, C.D., 2014. Contrasting the direct radiative effect and direct radiative forcing of aerosols. *Atmos. Chem. Phys.* 14 (11), 5513–5527. <http://dx.doi.org/10.5194/acp-14-5513-2014>.
- Holben, B.N., Tanré, D., Smirnov, A., Eck, T.F., Slutsker, I., Abuhassan, N., Newcomb, W.W., Schafer, J.S., Chatenet, B., Lavenu, F., Kaufman, Y.J., Castle, J.V., Setzer, A., Markham, B., Clark, D., Frouin, R., Halthore, R., Karneli, A., O'Neill, N.T., Pietras, C., Pinker, R.T., Voss, K., Zibordi, G., 2001. An emerging ground-based aerosol climatology: aerosol optical depth from AERONET. *J. Geophys. Res.* Atmos. 106 (D11), 12067–12097. <http://dx.doi.org/10.1029/2001JD900014>.
- Huang, K., Fu, J.S., Hsu, N.C., Gao, Y., Dong, X., Tsay, S.C., Lam, Y.F., 2013. Impact assessment of biomass burning on air quality in Southeast and East Asia during BASE-ASIA. *Atmos. Environ.* 78, 291–302. <http://dx.doi.org/10.1016/j.atmosenv.2012.03.048>.
- Huang, M., Carmichael, G.R., Kulkarni, S., Streets, D.G., Lu, Z., Zhang, Q., Pierce, R.B., Kondo, Y., Jimenez, J.L., Cubison, M.J., Anderson, B., Wisthaler, A., 2012. Sectoral and geographical contributions to summertime continental United States (CONUS) black carbon spatial distributions. *Atmos. Environ.* 51 (0), 165–174. <http://dx.doi.org/10.1016/j.atmosenv.2012.01.021>.
- Huang, X., Li, M., Li, J., Song, Y., 2012. A high-resolution emission inventory of crop burning in fields in China based on MODIS thermal anomalies/fire products. *Atmos. Environ.* 50 (0), 9–15. <http://dx.doi.org/10.1016/j.atmosenv.2012.01.017>.
- IPCC, 2013. *Climate Change 2013: the Physical Science Basis. Contribution of Working Group I to the Fifth Assessment Report of the Intergovernmental Panel on Climate Change.* Cambridge University Press, Cambridge, United Kingdom and New York, NY, USA, p. 1535.
- Janssens-Maenhout, G., Crippa, M., Guizzardi, D., Dentener, F., Muntean, M., Pouliot, G., Keating, T., Zhang, Q., Kurokawa, J., Wankmüller, R., Denier van der Gon, H., Klimont, Z., Frost, G., Darras, S., Koffi, B., 2015. HTAP_v2: a mosaic of regional and global emission gridded maps for 2008 and 2010 to study hemispheric transport of air pollution. *Atmos. Chem. Phys. Discuss.* 15 (8), 12867–12909. <http://dx.doi.org/10.5194/acpd-15-12867-2015>.
- Janssen, N.A.H., Gerlofs-Nijland, M.E., Lanki, T., Salonen, R.O., Cassee, F., Hoek, G., Fischer, P., Brunekreef, B., Krzyzanowski, M., 2012. *Health Effects of Black Carbon.* World Health Organization, Copenhagen.
- Jeong, J.L., Park, R.J., Woo, J.-H., Han, Y.-J., Yi, S.-M., 2011. Source contributions to carbonaceous aerosol concentrations in Korea. *Atmos. Environ.* 45 (5),

- 1116–1125. <http://dx.doi.org/10.1016/j.atmosenv.2010.11.031>.
- Jian, Y., Fu, T.M., 2014. Injection heights of springtime biomass-burning plumes over peninsular Southeast Asia and their impacts on long-range pollutant transport. *Atmos. Chem. Phys.* 14 (8), 3977–3989. <http://dx.doi.org/10.5194/acp-14-3977-2014>.
- Koch, D., Bond, T.C., Streets, D., Unger, N., van der Werf, G.R., 2007. Global impacts of aerosols from particular source regions and sectors. *J. Geophys. Res. Atmos.* 112 (D2), D02205. <http://dx.doi.org/10.1029/2005JD007024>.
- Kulkarni, S., Sobhani, N., Miller-Schulze, J.P., Shafer, M.M., Schauer, J.J., Solomon, P.A., Saide, P.E., Spak, S.N., Cheng, Y.F., Denier van der Gon, H.A.C., Lu, Z., Streets, D.G., Janssens-Maenhout, G., Wiedinmyer, C., Lantz, J., Artamonova, M., Chen, B., Imashev, S., Sverdluk, L., Deminter, J.T., Adhikary, B., D'Allura, A., Wei, C., Carmichael, G.R., 2014. Source sector and region contributions to BC and PM_{2.5} in Central Asia. *Atmos. Chem. Phys. Discuss.* 14 (8), 11343–11392. <http://dx.doi.org/10.5194/acpd-14-11343-2014>.
- Leibensperger, E.M., Mickley, L.J., Jacob, D.J., Chen, W.T., Seinfeld, J.H., Nenes, A., Adams, P.J., Streets, D.G., Kumar, N., Rind, D., 2012. Climatic effects of 1950–2050 changes in US anthropogenic aerosols—Part 1: aerosol trends and radiative forcing. *Atmos. Chem. Phys.* 12 (7), 3333–3348. <http://dx.doi.org/10.5194/acp-12-3333-2012>.
- Li, L.J., Wang, Y., Zhang, Q., Li, J.X., Yang, X.G., Jin, J., 2008. Wheat straw burning and its associated impacts on Beijing air quality. *Sci. China Ser. 51* (3), 1006–9313. <http://dx.doi.org/10.1007/s11430-008-0021-8>.
- Li, W.J., Shao, L.Y., Buseck, P.R., 2010. Haze types in Beijing and the influence of agricultural biomass burning. *Atmos. Chem. Phys.* 10 (17), 8119–8130. <http://dx.doi.org/10.5194/acp-10-8119-2010>.
- Li, Y., Cao, J.J., Zhang, X.Y., Che, H.Z., 2005. The variability and source apportionment of black carbon aerosol in Xi'an atmosphere during the autumn of 2003. *Clim. Environ. Res.* 10 (2), 229–237. <http://dx.doi.org/10.3878/j.issn.1006-9585.2005.02.10> (in Chinese).
- Liao, H., Seinfeld, J.H., 1998. Effect of clouds on direct aerosol radiative forcing of climate. *J. Geophys. Res. Atmos.* 103 (D4), 3781–3788. <http://dx.doi.org/10.1029/97JD03455>.
- Lin, C.Y., Zhao, C., Liu, X., Lin, N.H., Chen, W.N., 2014. Modelling of long-range transport of Southeast Asia biomass-burning aerosols to Taiwan and their radiative forcings over East Asia. *Tellus B* 66 (23733). <http://dx.doi.org/10.3402/tellusb.v66.23733>.
- Liu, H.Y., Jacob, D.J., Bey, I., Yantosca, R.M., 2001. Constraints from 210Pb and 7Be on wet deposition and transport in a global three-dimensional chemical tracer model driven by assimilated meteorological fields. *J. Geophys. Res. Atmos.* 106 (D11), 12109–12128. <http://dx.doi.org/10.1029/2000JD900839>.
- Liu, H.Y., Jacob, D.J., Bey, I., Yantosca, R.M., Duncan, B.N., Sachse, G.W., 2003. Transport pathways for Asian pollution outflow over the Pacific: interannual and seasonal variations. *J. Geophys. Res. Atmos.* 108 (D20), 8786. <http://dx.doi.org/10.1029/2002JD003102>.
- Lu, Z., Zhang, Q., Streets, D.G., 2011. Sulfur dioxide and primary carbonaceous aerosol emissions in China and India, 1996–2010. *Atmos. Chem. Phys.* 11 (18), 9839–9864. <http://dx.doi.org/10.5194/acp-11-9839-2011>.
- Lu, Z., Streets, D.G., Zhang, Q., Wang, S., 2012. A novel back-trajectory analysis of the origin of black carbon transported to the Himalayas and Tibetan Plateau during 1996–2010. *Geophys. Res. Lett.* 39 (1), L01809. <http://dx.doi.org/10.1029/2011GL049903>.
- Myhre, G., Berglen, T.F., Johnsrud, M., Hoyle, C.R., Bernsten, T.K., Christopher, S.A., Fahey, D.W., Isaksen, I.S.A., Jones, T.A., Kahn, R.A., Loebe, N., Quinn, P., Remer, L., Schwarz, J.P., Yttri, K.E., 2009. Modelled radiative forcing of the direct aerosol effect with multi-observation evaluation. *Atmos. Chem. Phys.* 9 (4), 1365–1392. <http://dx.doi.org/10.5194/acp-9-1365-2009>.
- Park, R.J., Jacob, D.J., Chin, M., Martin, R.V., 2003. Sources of carbonaceous aerosols over the United States and implications for natural visibility. *J. Geophys. Res. Atmos.* 108 (D12), 4355. <http://dx.doi.org/10.1029/2002JD003190>.
- Park, R.J., Jacob, D.J., Palmer, P.I., Clarke, A.D., Weber, R.J., Zondlo, M.A., Eisele, F.L., Bandy, A.R., Thornton, D.C., Sachse, G.W., Bond, T.C., 2005. Export efficiency of black carbon aerosol in continental outflow: global implications. *J. Geophys. Res. Atmos.* 110 (D11), D11205. <http://dx.doi.org/10.1029/2004JD005432>.
- Phadnis, M.J., Levy II, H., Moxim, W.J., 2002. On the evolution of pollution from South and Southeast Asia during the winter-spring monsoon. *J. Geophys. Res. Atmos.* 107 (D24), 4790. <http://dx.doi.org/10.1029/2002JD002190>.
- Qin, Y., Xie, S.D., 2012. Spatial and temporal variation of anthropogenic black carbon emissions in China for the period 1980–2009. *Atmos. Chem. Phys.* 12 (11), 4825–4841. <http://dx.doi.org/10.5194/acp-12-4825-2012>.
- Ramanathan, V., Carmichael, G., 2008. Global and regional climate changes due to black carbon. *Nat. Geosci.* 1 (4), 221–227. <http://dx.doi.org/10.1038/ngeo156>.
- Saikawa, E., Naik, V., Horowitz, L.W., Liu, J.F., Mauzerall, D.L., 2009. Present and potential future contributions of sulfate, black and organic carbon aerosols from China to global air quality, premature mortality and radiative forcing. *Atmos. Environ.* 43 (17), 2814–2822. <http://dx.doi.org/10.1016/j.atmosenv.2009.02.017>.
- Samset, B.H., Myhre, G., 2011. Vertical dependence of black carbon, sulphate and biomass burning aerosol radiative forcing. *Geophys. Res. Lett.* 38, L24802. <http://dx.doi.org/10.1029/2011GL049697>.
- Samset, B.H., Myhre, G., Schulz, M., Balkanski, Y., Bauer, S., Bernsten, T.K., Bian, H., Bellouin, N., Diehl, T., Easter, R.C., Ghan, S.J., Iversen, T., Kinne, S., Kirkevåg, A., Lamarque, J.F., Lin, G., Liu, X., Penner, J.E., Seland, Ø., Skeie, R.B., Stier, P., Takemura, T., Tsigaridis, K., Zhang, K., 2013. Black carbon vertical profiles strongly affect its radiative forcing uncertainty. *Atmos. Chem. Phys.* 13 (5), 2423–2434. <http://dx.doi.org/10.5194/acp-13-2423-2013>.
- Samset, B.H., Myhre, G., 2015. Climate response to externally mixed black carbon as a function of altitude. *J. Geophys. Res. Atmos.* 120, 2913–2927. <http://dx.doi.org/10.1002/2014JD022849>.
- Shindell, D., Lamarque, J.F., Unger, N., Koch, D., Faluvegi, G., Bauer, S., Ammann, M., Cofala, J., Teich, H., 2008. Climate forcing and air quality change due to regional emissions reductions by economic sector. *Atmos. Chem. Phys.* 8 (23), 7101–7113. <http://dx.doi.org/10.5194/acp-8-7101-2008>.
- Shindell, D., Kuylenstierna, J.C.I., Vignati, E., van Dingenen, R., Amann, M., Klimont, Z., Anenberg, S.C., Müller, N., Janssens-Maenhout, G., Raes, F., Schwartz, J., Faluvegi, G., Pozzoli, L., Kupiainen, K., Höglund-Isaksson, L., Emberson, L., Streets, D., Ramanathan, V., Hicks, K., Oanh, N.T.K., Milly, G., Williams, M., Demkina, V., Fowler, D., 2012. Simultaneously mitigating near-term climate change and improving human health and food security. *Science* 335 (6065), 183–189. <http://dx.doi.org/10.1126/science.1210026>.
- Smith, S.J., Mizrahi, A., 2013. Near-term climate mitigation by short-lived forcers. *Proc. Natl. Acad. Sci. U.S.A.* 110 (35), 14202–14206. <http://dx.doi.org/10.1073/pnas.1308470110>.
- Song, Y., Chang, D., Liu, B., Miao, W., Zhu, L., Zhang, Y., 2010. A new emission inventory for nonagricultural open fires in Asia from 2000 to 2009. *Environ. Res. Lett.* 5, 014014. <http://dx.doi.org/10.1088/1748-9326/5/1/014014>.
- Streets, D.G., Shindell, D.T., Lu, Z., Faluvegi, G., 2013. Radiative forcing due to major aerosol emitting sectors in China and India. *Geophys. Res. Lett.* 40 (16), 4409–4414. <http://dx.doi.org/10.1002/grl.50805>.
- Tao, J., Zhu, L.H., Han, J.L., Zhang, T., Chen, L.G., Xu, Z.C., 2009. Study on characteristics of black carbon aerosol pollution and preliminary exploration on its source in Guangzhou urban area during the winter. *Environ. Monit. China* 2, 53–56. <http://dx.doi.org/10.3969/j.issn.1002-6002.2009.02.019> (in Chinese).
- Unger, N., Shindell, D.T., Koch, D.M., Streets, D.G., 2008. Air pollution radiative forcing from specific emissions sectors at 2030. *J. Geophys. Res. Atmos.* 113 (D2), D02306. <http://dx.doi.org/10.1029/2007JD008683>.
- van der Werf, G.R., Randerson, J.T., Giglio, L., Collatz, G.J., Kasibhatla, P.S., Arellano Jr., A.F., 2006. Interannual variability in global biomass burning emissions from 1997 to 2004. *Atmos. Chem. Phys.* 6, 3423–3441. <http://dx.doi.org/10.5194/acp-6-3423-2006>.
- van der Werf, G.R., Randerson, J.T., Giglio, L., Collatz, G.J., Mu, M., Kasibhatla, P.S., Morton, D.C., DeFries, R.S., Jin, Y., van Leeuwen, T.T., 2010. Global fire emissions and the contribution of deforestation, savanna, forest, agricultural, and peat fires (1997–2009). *Atmos. Chem. Phys.* 10 (23), 11707–11735. <http://dx.doi.org/10.5194/acp-10-11707-2010>.
- Wang, J., Jacob, D.J., Martin, S.T., 2008. Sensitivity of sulfate direct climate forcing to the hysteresis of particle phase transitions. *J. Geophys. Res.* 113, D11207. <http://dx.doi.org/10.1029/2007JD009368>.
- Wang, Q., Jacob, D.J., Fisher, J.A., Mao, J., Leibensperger, E.M., Carouge, C.C., Le Sager, P., Kondo, Y., Jimenez, J.L., Cubison, M.J., Doherty, S.J., 2011. Sources of carbonaceous aerosols and deposited black carbon in the Arctic in winter-spring: implications for radiative forcing. *Atmos. Chem. Phys.* 11 (23), 12453–12473. <http://dx.doi.org/10.5194/acp-11-12453-2011>.
- Wang, Q., Jacob, D.J., Spackman, J.R., Perring, A.E., Schwarz, J.P., Moteki, N., Marais, E.A., Ge, C., Wang, J., Barrett, S.R.H., 2014. Global budget and radiative forcing of black carbon aerosol: constraints from pole-to-pole (HIPPO) observations across the Pacific. *J. Geophys. Res. Atmos.* 119 (1) <http://dx.doi.org/10.1002/2013JD020824>, 2013JD020824.
- Wang, R., Tao, S., Wang, W., Liu, J., Shen, H., Shen, G., Wang, B., Liu, X., Li, W., Huang, Y., Zhang, Y., Lu, Y., Chen, H., Chen, Y., Wang, C., Zhu, D., Wang, X., Li, B., Liu, W., Ma, J., 2012. Black carbon emissions in China from 1949 to 2050. *Environ. Sci. Technol.* 46 (14), 7595–7603. <http://dx.doi.org/10.1021/es3003684>.
- Wang, X., Wang, Y., Hao, J., Kondo, Y., Irwin, M., Munger, J.W., Zhao, Y., 2013. Top-down estimate of China's black carbon emissions using surface observations: sensitivity to observation representativeness and transport model error. *J. Geophys. Res. Atmos.* 118 (11), 5781–5795. <http://dx.doi.org/10.1002/jgrd.50397>.
- Wang, X., Heald, C.L., Ridley, D.A., Schwarz, J.P., Spackman, J.R., Perring, A.E., Coe, H., Liu, D., Clarke, A.D., 2014. Exploiting simultaneous observational constraints on mass and absorption to estimate the global direct radiative forcing of black carbon and brown carbon. *Atmos. Chem. Phys.* 14 (20), 10989–11010. <http://dx.doi.org/10.5194/acp-14-10989-2014>.
- Wesely, M.L., 1989. Parameterization of surface resistances to gaseous dry deposition in regional-scale numerical models. *Atmos. Environ.* 23 (6), 1293–1304. [http://dx.doi.org/10.1016/0004-6981\(89\)90153-4](http://dx.doi.org/10.1016/0004-6981(89)90153-4) (1967).
- Wu, J., Fu, C., Xu, Y., Tang, J.P., Wang, W., Wang, Z., 2008. Simulation of direct effects of black carbon aerosol on temperature and hydrological cycle in Asia by a Regional Climate Model. *Meteorol. Atmos. Phys.* 100 (1–4), 179–193. <http://dx.doi.org/10.1007/s00703-008-0302-y>.
- Zhang, L., Liao, H., Li, J., 2010. Impacts of Asian summer monsoon on seasonal and interannual variations of aerosols over eastern China. *J. Geophys. Res. Atmos.* 115 (D7), D00K05. <http://dx.doi.org/10.1029/2009JD012299>.
- Zhang, L., Henze, D.K., Grell, G.A., Carmichael, G.R., Bousseres, N., Zhang, Q., Cao, J., 2014. Constraining black carbon aerosol over Southeast Asia using OMI aerosol absorption optical depth and the adjoint of GEOS-Chem. *Atmos. Chem. Phys. Discuss.* 14, 28385–28452. <http://dx.doi.org/10.5194/acpd-14-28385-2014>.
- Zhang, Q., Streets, D.G., Carmichael, G.R., He, K.B., Huo, H., Kannari, A., Klimont, Z., Park, I.S., Reddy, S., Fu, J.S., Chen, D., Duan, L., Lei, Y., Wang, L.T., Yao, Z.L., 2009. Asian emissions in 2006 for the NASA INTEX-B mission. *Atmos. Chem. Phys.* 9 (14), 5131–5153. <http://dx.doi.org/10.5194/acp-9-5131-2009>.
- Zhang, X.Y., Wang, Y.Q., Zhang, X.C., Guo, W., Gong, S.L., 2008. Carbonaceous aerosol

- composition over various regions of China during 2006. *J. Geophys. Res. Atmos.* 113 (D14), D14111. <http://dx.doi.org/10.1029/2007JD009525>.
- Zhang, X.Y., Wang, Y.Q., Niu, T., Zhang, X.C., Gong, S.L., Zhang, Y.M., Sun, J.Y., 2012. Atmospheric aerosol compositions in China: spatial/temporal variability, chemical signature, regional haze distribution and comparisons with global aerosols. *Atmos. Chem. Phys.* 12, 779–799. <http://dx.doi.org/10.5194/acp-12-779-2012>.
- Zhang, Y.L., Huang, R.J., El Haddad, I., Ho, K.F., Cao, J.J., Han, Y., Zotter, P., Bozzetti, C., Daellenbach, K.R., Canonaco, F., Slowik, J.G., Salazar, G., Schwikowski, M., Schnelle-Kreis, J., Abbaszade, G., Zimmermann, R., Baltensperger, U., Prevot, A.S.H., Szidat, S., 2015. Fossil vs. non-fossil sources of fine carbonaceous aerosols in four Chinese cities during the extreme winter haze episode in 2013. *Atmos. Chem. Phys.* 15 (3), 1299–1312. <http://dx.doi.org/10.5194/acp-15-1299-2015>.
- Zheng, M., Salmon, L.G., Schauer, J.J., Zeng, L., Kiang, C.S., Zhang, Y., Cass, G.R., 2005. Seasonal trends in PM_{2.5} source contributions in Beijing, China. *Atmos. Environ.* 39 (22), 3967–3976. <http://dx.doi.org/10.1016/j.atmosenv.2005.03.036>.
- Zhuang, B.L., Jiang, F., Wang, T.J., Li, S., Zhu, B., 2011. Investigation on the direct radiative effect of fossil fuel black-carbon aerosol over China. *Theor. Appl. Climatol.* 104 (3–4), 301–312. <http://dx.doi.org/10.1007/s00704-010-0341-4>.
- Zhuang, B.L., Liu, Q., Wang, T.J., Yin, C.Q., Li, S., Xie, M., Jiang, F., Mao, H.T., 2013. Investigation on semi-direct and indirect climate effects of fossil fuel black carbon aerosol over China. *Theor. Appl. Climatol.* 114 (3–4), 651–672. <http://dx.doi.org/10.1007/s00704-013-0862-8>.
- Zhuang, B.L., Wang, T.J., Liu, J., Li, S., Xie, M., Yang, X.Q., Fu, C.B., Sun, J.N., Yin, C.Q., Liao, J.B., Zhu, J.L., Zhang, Y., 2014. Continuous measurement of black carbon aerosol in urban Nanjing of Yangtze River Delta, China. *Atmos. Environ.* 89 (0), 415–424. <http://dx.doi.org/10.1016/j.atmosenv.2014.02.052>.